

## A Model for the Spectral Albedo of Snow. I: Pure Snow

WARREN J. WISCOMBE AND STEPHEN G. WARREN<sup>1</sup>

National Center for Atmospheric Research,<sup>2</sup> Boulder, CO 80307

(Manuscript received 15 April 1980, in revised form 28 August 1980)

### ABSTRACT

We present a method for calculating the spectral albedo of snow which can be used at any wavelength in the solar spectrum and which accounts for diffusely or directly incident radiation at any zenith angle. For deep snow, the model contains only one adjustable parameter, an effective grain size, which is close to observed grain sizes. A second parameter, the liquid-equivalent depth, is required only for relatively thin snow.

In order for the model to make realistic predictions, it must account for the extreme anisotropy of scattering by snow particles. This is done by using the "delta-Eddington" approximation for multiple scattering, together with Mie theory for single scattering.

The spectral albedo from 0.3 to 5  $\mu\text{m}$  wavelength is examined as a function of the effective grain size, the solar zenith angle, the snowpack thickness, and the ratio of diffuse to direct solar incidence. The decrease in albedo due to snow aging can be mimicked by reasonable increases in grain size (50–100  $\mu\text{m}$  for new snow, growing to 1 mm for melting old snow).

The model agrees well with observations for wavelengths above 0.8  $\mu\text{m}$ . In the visible and near-UV, on the other hand, the model may predict albedos up to 15% higher than those which are actually observed. Increased grain size alone cannot lower the model albedo sufficiently to match these observations. It is also argued that the two major effects which are neglected in the model, namely nonsphericity of snow grains and near-field scattering, cannot be responsible for the discrepancy. Insufficient snow depth and error in measured absorption coefficient are also ruled out as the explanation. The remaining hypothesis is that visible snow albedo is reduced by trace amounts of absorptive impurities (Warren and Wiscombe, 1980, Part II).

### 1. Introduction

Radiation is the dominant component of the surface energy balance over snow during the melting season (Langleben, 1968; Weller, 1968; Paterson, 1969). Because the shortwave albedo of snow can fall from 90 to 50% or less, depending on snow condition, it controls the rate of melting. An ability to calculate snow albedo is therefore important for predicting seasonal snowmelt and runoff rates as well as for understanding the growth and decay of snowfields, which in turn affect the global energy budget and therefore climate (Kukla and Kukla, 1974). Furthermore, it may ultimately be necessary to calculate snow albedo in climate models (which now simply specify it) if the feedback between snow albedo and climate is to be understood.

We present here a simple analytical model for snow albedo. The model is useful for the entire solar spectrum (0.3–5  $\mu\text{m}$ ) and is based upon the delta-Eddington approximation (Joseph *et al.*, 1976)

for the bulk radiative transfer coupled with Mie calculations for the scattering by individual snow particles. The model uses no arbitrary adjustable parameters; the inputs are all observable quantities. It calculates snow albedo at any wavelength as a function of snow grain size, solar zenith angle, ratio of diffuse to direct incident solar radiation, and, for a thin snow layer, as a function of snow layer thickness and albedo of the underlying surface. We compare our model results with selected observations of these effects.

### 2. Previous snow albedo models

Only a small number of snow albedo models have been put forward. This undoubtedly reflects a feeling that there are not very much high-quality data against which to check such a model, that some of the data are contradictory, and that therefore at best only a crude model is justified.

The first and most widely used model is that of Dunkle and Bevans (1956). They applied the Schuster two-stream approximation to a homogeneous slab of snow on which only diffuse radiation is incident. The model contains two tunable parameters, an absorption and a scattering coefficient, and consider-

<sup>1</sup> Present affiliation: Cooperative Institute for Research in Environmental Sciences, University of Colorado, Boulder 80309.

<sup>2</sup> The National Center for Atmospheric Research is sponsored by the National Science Foundation.

able effort has gone into finding either numbers or functional forms for these coefficients (e.g., Weller, 1969; Schwerdtfeger, 1969; Bergen, 1971, 1975; Schlatter, 1972; Grenfell, 1979). Choudhury and Chang (1979) used a two-stream theory together with the Sagan-Pollack approximation for single-scattering albedo, and a backscatter fraction (7.5%) independent of wavelength. Their dependence of albedo on particle size and wavelength was qualitatively similar to that shown by Dunkle and Bevens (1956, Fig. 3), but the actual particle size necessary to obtain a particular albedo value was as much as a factor of 4 different.

Giddings and LaChapelle (1961) put forward a diffusion or random-walk model. Their paper is considerably more sophisticated than that of Dunkle and Bevens, particularly as regards its analysis of the model's range of validity (they conclude that the model is excellent for albedos over 80% and poor for albedos under 60%); however, their model requires two tunable parameters and diffuse incidence and is not demonstrably superior to Dunkle and Bevan's model.

Barkstrom (1972) and Bohren and Barkstrom (1974) applied more modern radiative transfer techniques to the snow albedo problem. Barkstrom assumed the snowpack to be semi-infinite, grey, and isotropically scattering with only direct-beam incidence. He was then able to apply the semi-analytical solutions available for the isotropic scattering problem and show, among other things, an increase in albedo with solar zenith angle, as is found observationally.

Bohren and Barkstrom (1974) improved on this work by treating scattering from individual snow grains (assumed spherical) using geometrical optics in the limit of *small* absorption; this eliminated both the unrealistic isotropic scattering assumption and the need for tunable parameters. They then used certain scaling relations of van de Hulst to reduce the problem back to one of isotropic scattering. These authors also showed that refraction *through* snow grains, not reflection *from* them, is mainly responsible for snow albedo, a point which had not been understood by earlier authors like Dunkle and Bevens (1956) or Middleton and Mungall (1952). Berger (1979)<sup>3</sup> has altered Bohren and Barkstrom's treatment to calculate infrared snow emissivities by using the limit of geometric optics for *large* instead of small absorption.

In summary, it may be said that substantial progress has been made in modeling snow albedo, but that no single model is valid for all wavelengths and

for an arbitrary combination of diffuse and direct incidence. None of the models, except Bohren-Barkstrom, account for the strong forward scattering from snow grains in a satisfactory fashion. A simpler yet more general analytical model would clearly be desirable.

### 3. Observations

#### a. Snow albedo

Measured snow albedos are generally high (80–90%) in the near-UV and visible (0.3–0.7  $\mu\text{m}$ ) but start dropping off steeply with wavelength in the near-IR between 0.8 and 1.5  $\mu\text{m}$  and remain generally low for longer wavelengths. Local maxima in the albedo are found at 1.1, 1.3, 1.8 and 2.2  $\mu\text{m}$ , corresponding to local minima in the absorption coefficient of ice. As snow ages with or without melting, the grain size increases and the albedo is reduced at all wavelengths.

Most field measurements have been made for spectrally averaged (all-wave) albedo, and the few spectral measurements, until very recently, have been for visible wavelengths only. Many of the latter have recently been reviewed by Mellor (1977, see our Fig. 16 which was taken from his paper). These measurements are not in agreement and in some cases are contradictory; a few are clearly wrong in their wavelength dependence. The better measurements show albedo to be fairly constant between 0.4 and 0.7  $\mu\text{m}$  wavelength. Sauberer (1938), Liljequist (1956) and Holmgren (1971) all find albedo to peak between 0.4 and 0.6  $\mu\text{m}$ , but disagree on the absolute value of albedo. Mellor (1977, Fig. 37) measured albedo to be erratic but generally decreasing with wavelength for  $0.4 \leq \lambda \leq 0.7 \mu\text{m}$ . Liljequist's Antarctic snow was clean, dry and fine-grained and his measurements represent a probable upper limit for snow albedo.

Whereas Holmgren and Liljequist measured albedo only at four discrete wavelengths, recent measurements with high spectral resolution have been reported for a variety of snow conditions in the Arctic Ocean by Grenfell and Maykut (1977) for  $0.4 \leq \lambda \leq 1.0 \mu\text{m}$ , and for dry snow in Antarctica by Kuhn and Siogas (1978) for  $0.4 \leq \lambda \leq 1.55 \mu\text{m}$ . Spectrally detailed measurements of bidirectional reflectance in the red and near-IR region ( $0.6 \leq \lambda \leq 2.5 \mu\text{m}$ ) have been reported by O'Brien and Munis (1975),<sup>4</sup> and for the near-UV ( $0.2 \leq \lambda \leq 0.45 \mu\text{m}$ ) by O'Brien (1977).<sup>5</sup>

<sup>3</sup> Berger, R. H., 1979: Snowpack optical properties in the infrared. CRREL Rep. 79-11, U.S. Army Cold Region Research and Engineering Lab, Hanover, NH. [NTIS AD-A071 004/6GAJ].

<sup>4</sup> O'Brien, H. W., and R. H. Munis, 1975: Red and near-infrared spectral reflectance of snow. CRREL Res. Rep. 332, 18 pp. [NTIS AD-A007 732/1GI].

<sup>5</sup> O'Brien, H. W., 1977: Observations of the ultraviolet spectral reflectance of snow. CRREL Rep. 77-27, 19 pp. [NTIS AD-A046 349/7GI].

Investigations have been made of the effects on snow albedo of individual parameters: solar zenith angle, cloud cover, snow age, snow depth, snow density and dust content. The albedo is found to increase as solar zenith increases, as measured on the Juneau Ice Field by Hubley (1955), on Arctic sea ice by Bryazgin and Koptev (1969), in the Rocky Mountains by Korff *et al.* (1974)<sup>6</sup> and on the Antarctic coast by Liljequist (1956) and Rusin (1961). Some workers, however, found the opposite trend. Havens (1964) reported highest albedos at midday, as did Kondratiev *et al.* (1964).

Cloud cover affects both the spectral distribution of irradiance and the effective zenith angle. It always causes an increase in the all-wave snow albedo. An increase of 5–10% relative to clear-sky albedo was found at Maudheim (Antarctica) by Liljequist (1956); 5–7% at the South Pole by Hanson (1960) and 11% at Mawson (Antarctica) by Weller (1968). Rusin's (1961) report is especially useful because he simultaneously measured cloud cover, solar zenith angle and all-wave albedo.

The effect of snow thickness on the albedo of a finite snowpack was reported for one wavelength ( $\lambda = 0.59 \mu\text{m}$ ) by Giddings and LaChapelle (1961). They found the snow albedo reaching its asymptotic value for depths larger than a few centimeters.

The reduction of spectral albedo due to snow aging has been investigated for visible wavelengths by Holmgren (1971) and Grenfell and Maykut (1977), and for the near-IR by O'Brien and Munis (1975).<sup>4</sup>

#### b. Snow grain size

Our snow albedo model, which assumes snow grains are spheres, is sensitive to the assumed value of average grain radius. Many observations have been made of the physical size of snow crystals and how their size increases with age, and many excellent photographs of individual snow crystals and grains are available (e.g., Nakaya, 1954; LaChapelle, 1969). But for a highly nonspherical snow crystal what is the average radius? The optical size may not be the same as the physical size, although snow crystals tend to be large enough that the two are nearly the same in the solar spectrum. Giddings and LaChapelle (1961) speculate that the appropriate average grain radius will be proportional to  $V/S$ , the volume-to-surface ratio. This may differ from our visual estimation of size, and it means that average grain radius will increase as a grain tends toward a sphere, even if its volume remains unchanged.

Fortunately for our modeling, snow crystals quickly lose their delicate shapes after falling. They may be broken up by the wind (Liljequist, 1956). They undergo "equitemperature metamorphism" (Sommerfeld and LaChapelle, 1970; Colbeck, 1979), in which water molecules migrate from one part of a crystal to another so as to reduce its surface free energy. This energy is proportional to  $S/V$ , which is least for a sphere; therefore, the crystals tend toward a spherical shape. Furthermore, since  $S/V$  is smaller for larger spheres, the larger spheres tend to grow at the expense of the smaller ones. Water molecules migrate faster the higher the temperature, and very rapidly indeed in snow at the melting point. Sooner or later, the snow grains become not only rounded but of fairly uniform size.

Grain size may vary by several factors with depth (e.g., Stephenson, 1967), but generally it is only the topmost 10–20 cm of snow which determine albedo, and in this region the grain size generally varies by less than 50%.

Snow grain metamorphism in Antarctica has been observed (Stephenson, 1967; Gow, 1969) to follow the same relationship as grain growth by sintering in metals and ceramics, *viz.*,

$$D^2 - D_0^2 = \alpha t e^{-\beta/T},$$

where  $D$  is grain diameter,  $t$  is time,  $T$  is Kelvin temperature, and  $\alpha$  and  $\beta$  are constants. This relationship offers the hope that our model will eventually be able to predict snow albedo as a function of age and temperature, rather than grain radius.

An examination of a wide variety of references (Nakaya, 1954; Liljequist, 1956; Arai, 1966; Colbeck, 1975; Gow, 1969; Hobbs, 1974; LaChapelle, 1969; Mellor, 1977; O'Brien and Munis, 1975,<sup>4</sup> Sommerfeld and LaChapelle, 1970; Stephenson, 1967) suggests average grain radii in the range 20–100  $\mu\text{m}$  for new snow, 100–300  $\mu\text{m}$  for fine-grained older snow, and 1.0–1.5 mm for old snow near the melting point. Therefore, in many of our examples, we shall use average grain radii of 50, 200 and 1000  $\mu\text{m}$  as representative of the range which exists in nature.

#### 4. Snow albedo model

Our approach was to design the simplest and most straightforward model possible, which would still be sophisticated enough to account for

- The wide variability in ice absorption with wavelength.
- The extremely forward-directed scattering from snow grains.
- An arbitrary mix of diffuse and direct radiation striking the snow surface.

<sup>6</sup> Korff, H. C., J. Gailiun and T. Vonder Haar, 1974: Radiation measurements over a snowfield at an elevated site. Atmos. Sci. Pap. No. 221, Colorado State University, [NTIS N74-31878/3GI].

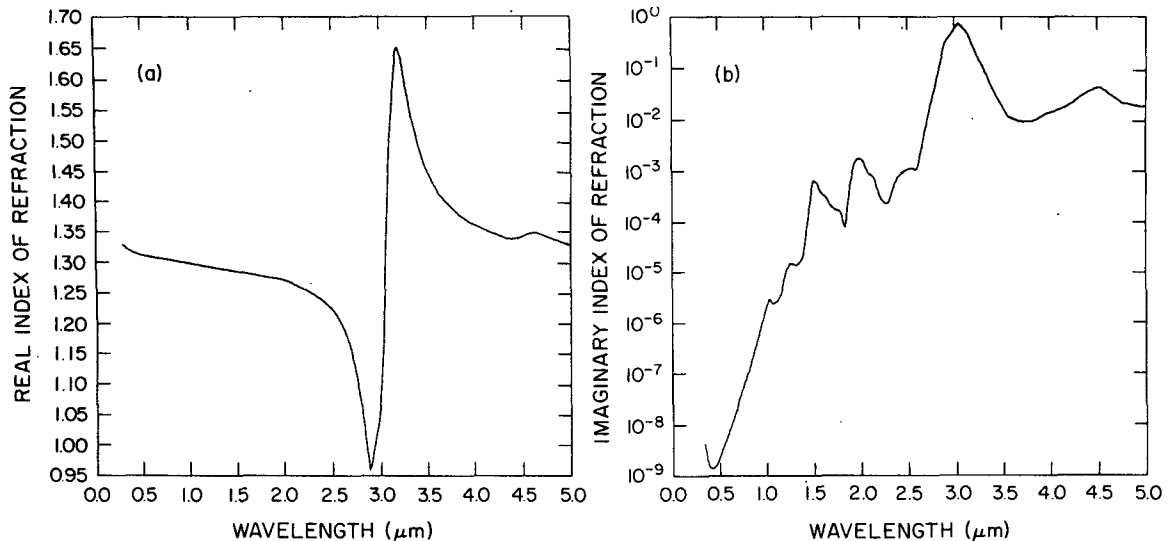


FIG. 1. Real and imaginary refractive index of ice at  $-7^{\circ}\text{C}$ , as a function of wavelength.

Previous models have been deficient in one or more of these areas (see Section 2). Our model depends on directly observable variables, rather than empirical or tunable parameters. These variables are

$m(\lambda)$	complex refractive index of ice [ $=m_{\text{re}}(\lambda) - im_{\text{im}}(\lambda)$ ]
$\lambda$	wavelength
$r$	mean snow grain radius
$\mu_0$	cosine of solar zenith angle $\theta_0$
$R$	ratio of diffuse incident flux to total (direct and diffuse) incident flux
$L$	equivalent depth of liquid water in snowpack ( $\text{g cm}^{-2}$ )
$A$	albedo of surface beneath snow.

The last two variables are only used if the snow is so thin that the underlying surface "shows through."  $L$  is obtained as the product  $\rho d$ , where  $\rho$  is the snow density ( $\text{g cm}^{-3}$ ) and  $d$  the snow thickness (cm). The ice volume absorption coefficient is

$$\beta_{\text{abs}} = 4\pi\lambda^{-1}m_{\text{im}}(\lambda)$$

and assumes the same units as  $\lambda^{-1}$ . This relation has been used to deduce  $m_{\text{im}}$  from measured values of  $\beta_{\text{abs}}$  in some spectral regions.

#### a. Ice refractive index

The careful measurements of ice refractive index at  $-7^{\circ}\text{C}$  by Schaaf and Williams (1973) are used for the real refractive index  $m_{\text{re}}(\lambda)$  when  $\lambda \geq 2 \mu\text{m}$  and for the imaginary index  $m_{\text{im}}(\lambda)$ ,  $\lambda \geq 2.77 \mu\text{m}$ . For other wavelengths we employed a congeries of sources to be described below. Our deduced refractive index values are plotted in Fig. 1 from  $\lambda = 0.30$  to  $5 \mu\text{m}$ . (Radiation at wavelengths  $< 0.30$

$\mu\text{m}$  does not reach the surface.) A tabular rendition of Fig. 1 is available from the authors.

Linear interpolation was used to obtain values of  $m_{\text{re}}(\lambda)$  at wavelengths between those where measurements were available. The actual procedures used to obtain  $m_{\text{re}}(\lambda)$  in the various wavelength intervals were as follows:

1) 0.3–0.4  $\mu\text{m}$ : Linear extrapolation from Hobbs' (1974) Table 3.1.

2) 0.4–0.55  $\mu\text{m}$ : Hobbs' (1974) Table 3.1 gives two values of  $m_{\text{re}}$ , one for the ordinary ray ( $m_{\text{re}}^o$ ) and one for the extraordinary ray ( $m_{\text{re}}^e$ ), which differ only slightly because ice birefringence is small; these are weighted by the fraction of energy going into each ray and averaged,  $m_{\text{re}} = \frac{2}{3}m_{\text{re}}^o + \frac{1}{3}m_{\text{re}}^e$ .

3) 0.55–2  $\mu\text{m}$ : Linear interpolation between Hobbs' value at 0.55  $\mu\text{m}$  and Schaaf and Williams' value at 2.0  $\mu\text{m}$ , which differ by only 0.04 so that the error incurred by this long interpolation should be of little consequence. Earlier measurements by Bode (1909) and Kislovskii (1959), as reworked by Irvine and Pollack (1968), disagree with Schaaf and Williams in the region where they overlap, and so we reject them. (Irvine and Pollack admit that their sources are unreliable for  $1 \leq \lambda \leq 3 \mu\text{m}$ .)

For the  $m_{\text{im}}(\lambda)$  values in Fig. 1, we performed logarithmic interpolation (assuming  $\ln m_{\text{im}}$  to be linear in  $\lambda$ ) between available measurements. Measurements in the region 1.40–2.65  $\mu\text{m}$  were corrected to  $-7^{\circ}\text{C}$  using the temperature dependences of Irvine and Pollack [1968, Eq. (1) and Table 3]. (The temperature dependence is quite small.) Our detailed procedures for the various wavelength intervals were as follows:

4) 0.3–0.313  $\mu\text{m}$ : Logarithmic extrapolation from

Sauberer's (1950) value at  $0.313 \mu\text{m}$ , using the trend of the  $m_{\text{im}}(\lambda)$  curve for liquid water (Irvine and Pollack, 1968, Fig. 1a) as a guide.

5)  $0.313\text{--}0.80 \mu\text{m}$ : Sauberer's (1950) measurements of light transmission through 15–50 cm thick plane-shaven blocks of clean bubble-free lake ice. His assumption of a 4% reflection loss at the plane interfaces is a modest overestimate of the calculated Fresnel reflectance at normal incidence, but the corrected absorption coefficients would be at most a factor of 1.4 greater and this turned out to have a negligible effect on our calculated snow albedos at these wavelengths. Sauberer noted that his absorption coefficients were roughly an order of magnitude smaller than those of Kalitin (1936), who also used lake ice. The measurements of ice absorption in this spectral region are more uncertain than in almost any other, because of the long path lengths of pure ice required and because of possible scattering from microbubbles. Comparison with the more carefully measured curves for water (Hale and Querry, 1973; Palmer and Williams, 1974) reveal much more structure around 0.6, 0.75 and  $0.97 \mu\text{m}$  than Sauberer found in the ice curves, and because of the structural similarities between the water and ice curves in other spectral regions, one strongly suspects that the ice curves have just not been measured well enough from 0.3 to  $1 \mu\text{m}$ .

6)  $0.80\text{--}0.95 \mu\text{m}$ : Logarithmic interpolation from Sauberer's (1950) "visible series" measurement at  $0.80 \mu\text{m}$  to Luck's (1963) measurement at  $0.95 \mu\text{m}$ . The Luck value is the one favored by Irvine and Pollack (1968), who quote no values of  $m_{\text{im}}(\lambda)$  below  $\lambda = 0.95 \mu\text{m}$ . Sauberer made measurements within this spectral region but cautioned that the values were order-of-magnitude only. They deviate typically by 20% from Luck's values for  $0.95\text{--}1.1 \mu\text{m}$  and even more than that from Sauberer's own "visible series" value at  $0.8 \mu\text{m}$ , so we have ignored them. While Lyons and Stoiber (1959) give an excellent critical review of previous measurements, we chose not to use their measurements for this region because they are lower than Luck's by a factor of 2 or so.

7)  $0.95\text{--}2.65 \mu\text{m}$ : Based on Irvine and Pollack's (1968) recommendations, we used Luck (1963) for  $0.95\text{--}1.30 \mu\text{m}$ , Ockman (1958) for  $1.40 \mu\text{m}$  and  $1.9\text{--}2.1 \mu\text{m}$ , and Reding (1951) for  $1.45\text{--}1.85 \mu\text{m}$  and  $2.15\text{--}2.65 \mu\text{m}$ . The largest uncertainty is near  $1.85 \mu\text{m}$ , where neither Reding's nor Ockman's values are reliable because transmissions through their ice samples were close to 100%. Reding's sample thickness was also poorly determined. Use of his value at  $1.85 \mu\text{m}$  leads to poor agreement between our model and observed snow albedo just near that wavelength (Ockman's value gives an equal disagreement in the opposite direction.)

8)  $2.65\text{--}2.77 \mu\text{m}$ : Logarithmic interpolation between Schaaf and Williams' value at  $2.77 \mu\text{m}$  and Reding's value at  $2.65 \mu\text{m}$ .

#### b. Scattering by individual snow grains

We have assumed the individual snow grains scatter like spheres in each other's far fields (we discuss the relaxation of the far-field assumption in Section 7). In reality, of course, snow grains are not exactly spherical, but there are still several compelling reasons for assuming sphericity (reviewed by Mugnai and Wiscombe, 1980). The possible effects of nonsphericity on snow albedo are discussed in Section 7b.

The formulas for scattering by spheres are reviewed by van de Hulst (1957). They require as input the dimensionless size parameter  $x = 2\pi r/\lambda$  and the complex refractive index  $m(\lambda)$ . We require as output the three quantities:

$\sigma_{\text{ext}} = \pi r^2 Q_{\text{ext}} =$  extinction cross section,

$\bar{\omega} = \frac{\sigma_{\text{scat}}}{\sigma_{\text{ext}}} =$  single-scatter albedo (ratio of scattering to extinction cross-section),

$g =$  asymmetry factor (mean value of  $\cos\theta$ , where  $\theta$  is scattering angle).

The first quantity  $\sigma_{\text{ext}}$  is required only when the snow layer is *not* optically semi-infinite;  $Q_{\text{ext}}$  is the dimensionless "extinction efficiency." Both  $\bar{\omega}$  and  $g$  are dimensionless with ranges  $0 \leq \bar{\omega} \leq 1$  and  $-1 \leq g \leq 1$ .  $g = 0$  corresponds to isotropic scattering and  $g = 1$  to completely forward-directed scattering. Plots of the variations of  $Q_{\text{ext}}$ ,  $\bar{\omega}$  and  $g$  with  $x$  and with  $m(\lambda)$  may be found in the review paper of Hansen and Travis (1974).

All three quantities,  $Q_{\text{ext}}$ ,  $\bar{\omega}$  and  $g$ , approach definite geometric-optics limits as  $x \rightarrow \infty$  (e.g.,  $Q_{\text{ext}} \rightarrow 2$ ), albeit at different rates. But even though  $x > 50$  and more typically  $x \gg 50$  for snow grains in the solar spectrum, we found that the actual geometric-optics limiting values were *not* always accurate enough, especially in the near infrared and for the smaller grain sizes. Therefore, we calculated the exact spherical Mie results using the fast algorithms of Wiscombe (1979, 1980). However, Mie quantities as a function of  $x$  contain a quasi-oscillatory "ripple" which causes erratic fluctuations in the spectral albedo curves. Such fluctuations are unrealistic because there is always a sufficient range of grain sizes in snow to eliminate them. We have eliminated the ripple by averaging over a range of sizes which is small relative to the mean grain size.

Figs. 2–4 show our calculated values of  $Q_{\text{ext}}$ ,  $1 - \bar{\omega}$ , and  $g$  as a function of wavelength across the solar spectrum ( $0.3\text{--}5.0 \mu\text{m}$ ).  $Q_{\text{ext}}$  and  $g$  are rela-

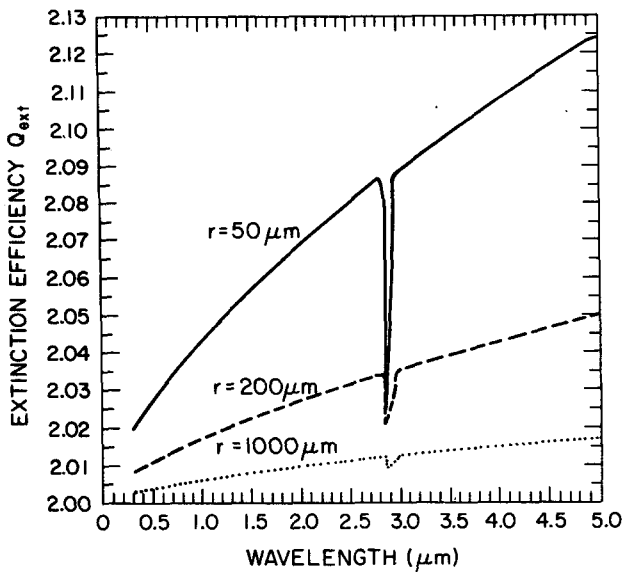


FIG. 2. Extinction efficiency ( $Q_{ext}$ ) for ice spheres of various radii, as a function of wavelength.

tively weak functions of wavelength compared to  $1 - \bar{\omega}$ , and so we shall find later that the spectral variation of snow albedo is caused almost exclusively by  $1 - \bar{\omega}$ .

In Fig. 2 we see that the larger the grain radius, the closer  $Q_{ext}$  is to its geometric-optics value of 2. It departs increasingly from 2 as wavelength increases, although even for 50  $\mu\text{m}$  grains at  $\lambda = 5 \mu\text{m}$  the departure is only 6%. The sharp dips at the 3  $\mu\text{m}$  absorption edge, where  $m_{re} \rightarrow 1$ , occur because the

Fresnel reflectances at the surface of the sphere nearly vanish there, virtually eliminating the reflection contribution to  $Q_{ext}$ .

The coalbedo  $1 - \bar{\omega}$  (Fig. 3) rises fairly monotonically from values in the neighborhood of  $10^{-5}$  in the visible to values between 0.1 and 0.5 at  $\lambda = 1.5 \mu\text{m}$ . The upper limit is  $\sim 0.5$  rather than 1.0, for reasons explained in Hansen and Travis (1974); as a consequence there is always some scattering, and the snow albedo will never strictly go to zero, although it does dip to values between 0.1 and 1% in the regions of strongest absorption. Beyond  $\lambda = 1.5 \mu\text{m}$  the coalbedo is plotted on a linear scale and can be seen to undergo large variations as a consequence of the various ice absorption bands in Fig. 1. Near  $\lambda = 3 \mu\text{m}$ , where ice absorption is maximal ( $m_{im} \approx 1$ ), one begins to enter the "mirror-reflection" regime typical of highly-conducting metals, and here  $1 - \bar{\omega}$  actually decreases as  $m_{im}$  increases. Later we shall see that this produces a seemingly paradoxical local maximum in snow albedo just past  $\lambda = 3 \mu\text{m}$ .

The asymmetry factor  $g$  (Fig. 4) assumes values in the fairly narrow range 0.88 to 1.0, with smaller and fairly uniform values across the visible, and larger and more variable values across the near infrared. It rises to  $\sim 0.997$  at the 3  $\mu\text{m}$  absorption edge, which is due to the aforementioned vanishing of the reflection contribution to scattering (leaving only diffraction). Even though the values of  $g$  are rather restricted in range, the snow albedo is distinctly affected by it since mean photon path lengths in the snow are sensitive functions of  $g$ , being longer, the larger  $g$  is.

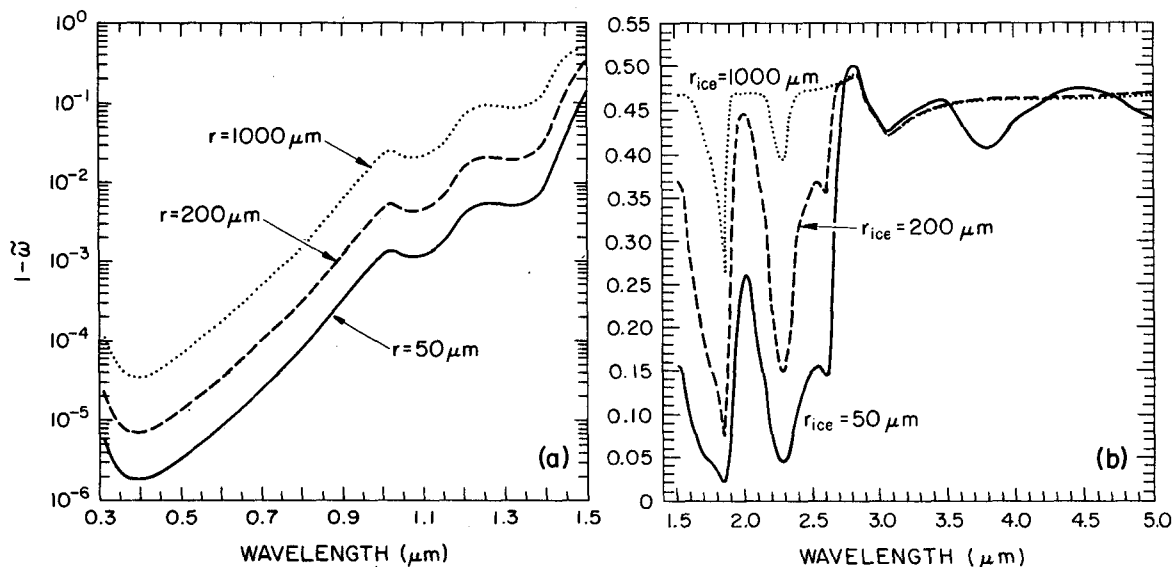


FIG. 3. Single-scattering coalbedo ( $1 - \bar{\omega}$ ) for ice spheres of various radii, as a function of wavelength.

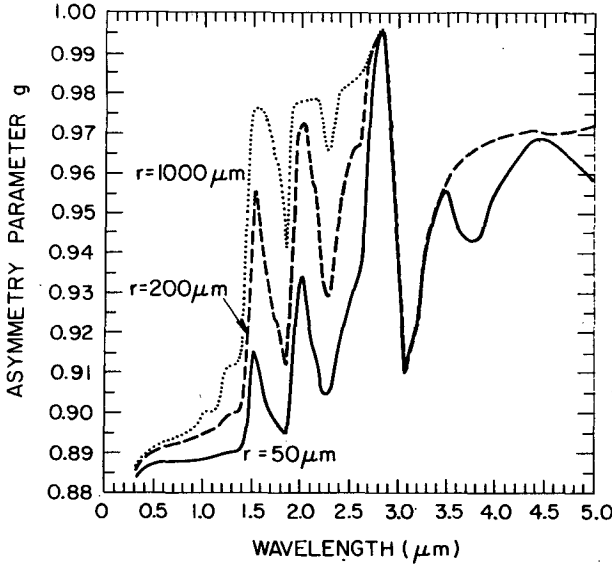


FIG. 4. Asymmetry factor  $g$  for ice spheres of various radii, as a function of wavelength.

The sharp spikes near  $\lambda = 1.85 \mu\text{m}$  in both the  $g$  and  $1 - \bar{\omega}$  plots are produced by values of ice imaginary index which, as noted previously, we consider unreliable.

### c. Multiple scattering in the snowpack

The radiative transfer model which best fulfilled the stipulations at the beginning of this section was, we felt, the delta-Eddington approximation (Joseph *et al.*, 1976). It was designed specifically to handle strongly forward-directed scattering (i.e.,  $0.6 \leq g < 1$ ) such as we have in the case of a snowpack. As further demonstrated by Wiscombe and Joseph (1977), it is a good approximation over the complete ranges of  $\bar{\omega}$ ,  $g$ , and snow optical depth

$$\tau_0 = N\sigma_{\text{ext}}d = \frac{L\sigma_{\text{ext}}}{\frac{4}{3}\pi r^3\rho_{\text{ice}}} = \frac{3LQ_{\text{ext}}}{4r\rho_{\text{ice}}}, \quad (1)$$

where  $N$  is number density of snow grains and  $\rho_{\text{ice}}$  is the density of pure ice ( $0.917 \text{ g cm}^{-3}$ ). The delta-Eddington approximation is capable of accounting for direct-beam as well as diffuse incidence on the snowpack, or any arbitrary mixture of the two. Thus we are able to eliminate a number of the restrictions inherent in some of the earlier multiple-scattering models for snow (Section 2).

The delta-Eddington approximation begins by transforming the three fundamental variables  $\tau_0$ ,  $\bar{\omega}$ , and  $g$  as follows:

$$g^* = \frac{g}{1 + g}, \quad (2a)$$

$$\bar{\omega}^* = \frac{(1 - g^2)\bar{\omega}}{1 - g^2\bar{\omega}}, \quad (2b)$$

$$\tau_0^* = (1 - \bar{\omega}g^2)\tau_0. \quad (2c)$$

Then the ordinary Eddington approximation is applied to a layer described by  $\tau_0^*$ ,  $\bar{\omega}^*$  and  $g^*$ . Note that this new fictitious layer is much less forward scattering ( $g^* < 1/2$ ), more absorptive ( $\bar{\omega}^* < \bar{\omega}$ ), but less optically thick ( $\tau_0^* < \tau_0$ ) in just the right proportion that the absorption part of the layer optical depth is unaltered. Only the scattering optical depth is reduced.

Note that when  $\bar{\omega}$  is near unity (in the  $0.3\text{--}1.0 \mu\text{m}$  wavelength region for snow), one has  $\tau_0^* \approx 0.2\tau_0$ , which means that it takes a five times larger depth of snow to be effectively semi-infinite at these wavelengths than it would if snow were an isotropic scatterer.

Let us first assume that only a direct beam is incident at zenith angle  $\theta_0 = \cos^{-1}\mu_0$ . Assume further a diffusely-reflecting surface of albedo  $A$  below the snowpack. The delta-Eddington formula for the snowpack albedo  $a_s$  in this case is

$$\begin{aligned} Qa_s(\mu_0) &= 2 \left[ P(1 - \gamma + \bar{\omega}^*b^*) + \bar{\omega}^*(1 + b^*) \frac{\gamma\xi\mu_0 - P}{1 - \xi^2\mu_0^2} \right] \\ &\times \exp(-\tau_0^*/\mu_0) - \bar{\omega}^*b^*(Q^+ - Q^-) \\ &+ \bar{\omega}^*(1 + b^*) \left( \frac{Q^+}{1 + \xi\mu_0} - \frac{Q^-}{1 - \xi\mu_0} \right), \quad (3) \end{aligned}$$

where

$$a^* = 1 - \bar{\omega}^*g^*,$$

$$b^* = g^*/a^*,$$

$$\xi = [3a^*(1 - \bar{\omega}^*)]^{1/2},$$

$$P = 2\xi/(3a^*),$$

$$\gamma = (1 - A)/(1 + A),$$

$$Q^\pm = (\gamma \pm P) \exp(\pm \xi\tau_0^*),$$

$$Q = (1 + P)Q^+ - (1 - P)Q^-.$$

The formula for  $a_s(\mu_0)$  has been written in order to display the entire  $\mu_0$ -dependence explicitly, with a view to later integration over  $\mu_0$ . For  $\bar{\omega}^* = 1$ , there is a removable singularity (of the form  $0/0$ ); but for a snowpack the nonabsorbing  $\bar{\omega}^* = 1$  case never occurs, otherwise albedos of 100% would be observed. And the formula (3) is well-behaved computationally even for  $\bar{\omega}^*$  very near 1, because  $\xi$  (and therefore  $P$ ) go to zero only as  $(1 - \bar{\omega}^*)^{1/2}$ , which is a much larger quantity than  $(1 - \bar{\omega}^*)$  itself. The formula has another removable singularity at  $\mu_0 = 1/\xi$  if  $\xi \geq 1$ , which can only occur if  $\omega^*$

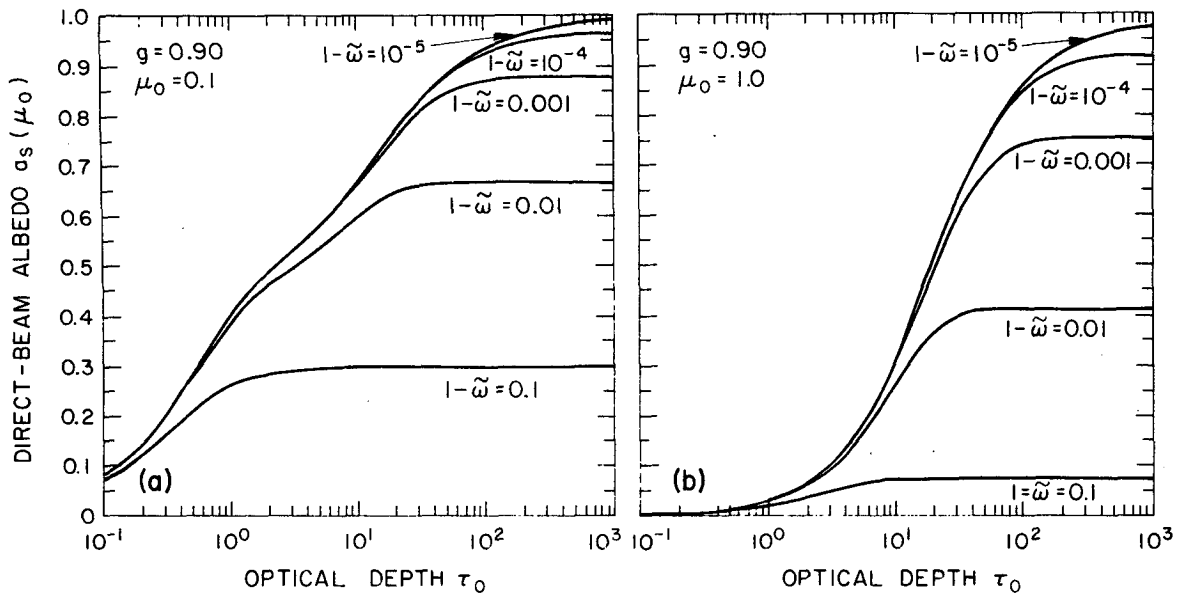


FIG. 5. Direct-beam albedo  $a_s^\infty(\mu_0)$  versus snowpack optical thickness  $\tau_0$  for various values of single-scattering coalbedo ( $1 - \bar{\omega}$ ).

$< \frac{2}{3}$ ; this singularity requires special attention when integrating  $a_s(\mu_0)$  over  $\mu_0$  analytically.

Fig. 5 shows  $a_s(\mu_0)$  as a function of optical depth  $\tau_0$  of the snowpack for a black underlying surface ( $A = 0$ ). A typical value  $g = 0.9$  is taken for the asymmetry factor, and extreme cases of near-grazing incidence ( $\mu_0 = 0.1$ ) and normal incidence ( $\mu_0 = 1.0$ ) are shown. The approach of  $a_s(\mu_0)$  to its semi-infinite ( $\tau_0 \rightarrow \infty$ ) value

$$a_s^\infty(\mu_0) = \frac{\bar{\omega}^*}{1 + P} \frac{1 - b^* \xi \mu_0}{1 + \xi \mu_0} \quad (4)$$

is slower and slower, the smaller  $1 - \bar{\omega}$  is.  $\tau_0 = 7$  is effectively semi-infinite for  $1 - \bar{\omega} = 0.1$ , while for  $1 - \bar{\omega} = 10^{-5}$  the semi-infinite limit has barely been attained at  $\tau_0 = 1000$ . Thus Fig. 3 and Fig. 5 together show that infinitesimal depths of snow are effectively semi-infinite at near infrared wavelengths, while depths at least two orders of magnitude larger are required at visible wavelengths (this point is discussed further in Section 5e). By comparing the two parts of Fig. 5, one can see that the sun angle ( $\mu_0$ ) effect is strongest at the smaller optical depths and becomes weaker as optical depth increases.

The sun angle dependence is much weaker in the visible (small  $1 - \bar{\omega}$ ) cases than in the near infrared cases, which can be seen in Fig. 6 where  $a_s^\infty(\mu_0)$  is plotted versus  $\mu_0$  for  $g = 0.90$ . The  $\mu_0$  dependence is so weak for the visible cases ( $1 - \bar{\omega} = 10^{-4}, 10^{-5}$ ) that it would be difficult to detect experimentally. Furthermore,  $a_s^\infty(\mu_0)$  is almost perfectly linear in

$\mu_0$  for  $1 - \bar{\omega}$  up to  $10^{-3}$ , and fairly linear even up to  $1 - \bar{\omega} = 0.1$ .

Observations of the sun-angle dependence of snow albedo by Hubley (1955), Liljequist (1956), Rusin (1961), Bryazgin and Koptev (1969), and Korff

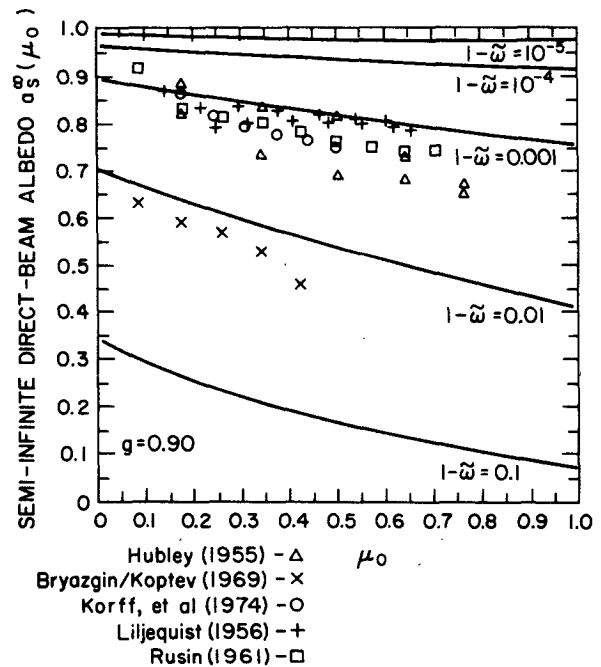


FIG. 6. Semi-infinite direct beam albedo  $a_s^\infty(\mu_0)$  versus cosine of direct-beam zenith angle  $\mu_0$ , for several values of single-scattering coalbedo ( $1 - \bar{\omega}$ ).

*et al.* (1974)<sup>6</sup> are also plotted on Fig. 6. The Bryazgin/Koptev measurements refer to a 0.6–1.2  $\mu\text{m}$  wavelength interval, and are best fitted by the  $1 - \tilde{\omega} = 0.01$  curve; from Fig. 3, however, it appears that  $1 - \tilde{\omega} = 0.001$  is a more appropriate mean value for this wavelength interval. The reason for this discrepancy is not clear, but may be due to the presence of impurities (see Part II). The remaining measurements refer to the whole solar spectrum and are very roughly fitted by the  $1 - \tilde{\omega} = 0.001$  curve since the mean value of  $g$  (see Fig. 4) is between 0.9 and 0.95. All except the measurements of Hubley tend to be in rough agreement with our predicted  $\mu_0$ -dependence; but as Hubley himself notes, there is considerable disagreement in the literature over the nature of this dependence, and his measurements seem to exhibit a stronger  $\mu_0$  dependence than subsequent investigators have found.

Under overcast skies the incident flux will be diffuse rather than direct. It is possible to derive a simple formula for the albedo in this case by applying a diffuse-flux upper boundary condition to the delta-Eddington equations, but Wiscombe (1977) has shown that this formula sometimes yields negative albedos, *especially* for the semi-infinite case of most interest for snow. Therefore, we prefer to get the diffuse albedo  $a_d$  by assuming isotropically incident radiation and integrating the direct-beam albedo (3) over all angles of incidence:

$$a_d = 2 \int_0^1 \mu_0 a_s(\mu_0) d\mu_0. \quad (5)$$

This will always be positive because it can be shown that  $a_s(\mu_0)$  is always positive. Putting (3) into (5) and performing some rather lengthy manipulations leads to

$$\begin{aligned} Qa_d = 2P \left[ (1 - \gamma + \tilde{\omega}^* b^*)(1 - \tau_0^*) - \frac{\gamma \tilde{\omega}^*(1 + b^*)}{1 - \tilde{\omega}^*} \right] \exp(-\tau_0^*) - 2P \left[ \tilde{\omega}^*(1 + b^*) \left( \frac{2}{\xi^2} + \frac{\gamma \tau_0^*}{1 - \tilde{\omega}^*} \right) \right. \\ \left. + (1 - \gamma + \tilde{\omega}^* b^*) \tau_0^{*2} \right] \text{Ei}(-\tau_0^*) + \frac{2\tilde{\omega}^*(1 + b^*)}{\xi^2} \left[ Q^+ \{ \text{Ei}[-(1 + \xi)\tau_0^*] + \xi - \ln(1 + \xi) \} \right. \\ \left. - Q^- \{ \text{Ei}[-(1 - \xi)\tau_0^*] - \xi - \ln|1 - \xi| \} \right] - \tilde{\omega}^* b^* (Q^+ - Q^-), \quad (6) \end{aligned}$$

where Ei is the exponential integral:

$$\text{Ei}(x) = \begin{cases} - \int_{-x}^{\infty} e^{-t} t^{-1} dt, & x < 0 \\ - \lim_{\epsilon \rightarrow 0^+} \left[ \int_{-x}^{-\epsilon} + \int_{\epsilon}^{\infty} \right] e^{-t} t^{-1} dt, & x > 0. \end{cases}$$

The upper definition of Ei( $x$ ) is equivalent to  $-E_1(-x)$  (cf. Abramowitz and Stegun, 1965, p. 228) and the lower definition is the Cauchy principal value of the same integral. This same Cauchy principal value also is used to evaluate the integral leading to the  $\ln|1 - \xi|$  term when  $\xi > 1$ . Note that the expression in braces containing  $\ln|1 - \xi|$  is finite as  $\xi \rightarrow 1$  even though  $\ln|1 - \xi|$  blows up in that limit.

One finds diffuse albedo equal to direct albedo ( $a_d = a_s$ ) at any optical depth for  $\mu_0 = 0.6$ – $0.7$ , corresponding to solar elevations between 37 and 44°. This conclusion is quite insensitive to asymmetry factor in the expected range ( $g = 0.8$ – $1.0$ ) for snow. Thus the formation of cloud cover over snow should raise its spectral albedo for solar elevations exceeding  $\sim 40^\circ$  and lower it for solar elevations below  $40^\circ$ .

In the semi-infinite limit the diffuse albedo becomes

$$a_d^\infty = \frac{2\tilde{\omega}^*}{1 + P} \left\{ \frac{1 + b^*}{\xi^2} [\xi - \ln(1 + \xi)] - b^*/2 \right\}. \quad (7)$$

In Fig. 7,  $a_d^\infty$  is plotted versus  $1 - \tilde{\omega}$  for several values of  $g$  relevant to snow. One sees that for the small values of  $1 - \tilde{\omega}$  typical of the visible,  $a_d^\infty$  is only weakly dependent on the asymmetry factor. For the larger values of  $1 - \tilde{\omega}$  typical of the near infrared,  $a_d^\infty$  exhibits considerably more sensitivity to  $g$ .

For a combination of direct and diffuse incident radiation with a diffuse fraction  $R$ , the net albedo predicted by the model is

$$a_{\text{net}} = R a_d + (1 - R) a_s(\mu_0). \quad (8)$$

## 5. Spectral albedo calculations for pure snow

The parameters which influence the albedo are grain size, solar zenith angle, ratio of diffuse to direct incident flux and snow layer thickness. We examine the effect of each of these parameters in turn, keeping the other parameters fixed at "standard" values of semi-infinite snow depth, 100  $\mu\text{m}$  grain radius, and direct solar radiation at  $60^\circ$  zenith angle incident on the snow surface. These standard conditions would be characteristic of a new-fallen

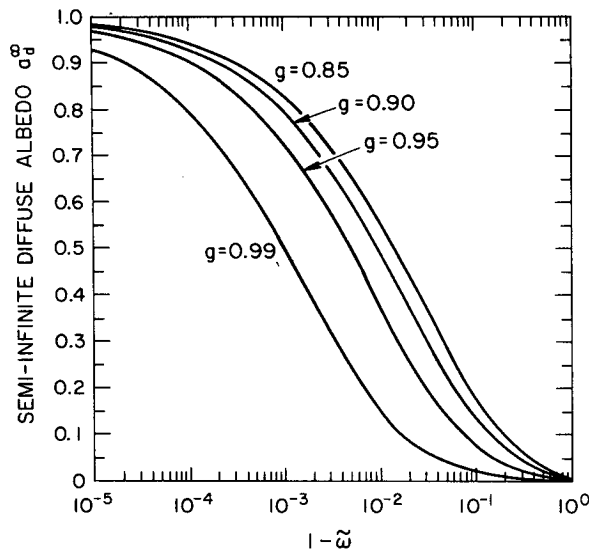


FIG. 7. Semi-infinite diffuse albedo  $a_d^\infty$  versus single-scattering coalbedo  $1 - \bar{\omega}$  for several values of asymmetry factor  $g$ .

snow pack deeper than 30 cm under clear skies, either in winter at midlatitudes or in spring and summer at high latitudes. We also investigate the sensitivity of our results to uncertainty in the reported absorption coefficient of ice.

It should be borne in mind that the spectrally integrated albedo is weighted by the solar spectral flux reaching the surface, so that failure to calculate correct albedo at short wavelengths is more serious than at longer wavelengths. The albedo is very low, 5% or less, for  $\lambda \geq 2.8 \mu\text{m}$ , so this spectral region will contribute practically nothing to the spectrally integrated snow albedo.

#### a. Dependence on grain size (or age)

Fig. 8 shows the spectral albedo for several values of the grain radius. The plotting increment is  $0.01 \mu\text{m}$  from  $0.3$  to  $2.8 \mu\text{m}$ , and beyond that just the wavelengths at which Schaaf and Williams (1973) measured ice imaginary index are used. Fig. 8b is plotted from  $2.8$  to  $12 \mu\text{m}$  wavelength on an expanded vertical scale to show the small but non-zero albedo values which obtain in that range. Since grain size generally increases as the snow ages, it is clear from this figure that the albedo falls at all wavelengths as the grain radius or the age increases. This is due to the fact that larger grains are both more absorptive and more forward scattering. But for  $\lambda < 2.5 \mu\text{m}$  the fall in albedo is primarily due to the decrease in  $\bar{\omega}$  (see Fig. 3); the increase in asymmetry factor (Fig. 4) is comparatively small. At  $\lambda = 1.3 \mu\text{m}$ , for example,  $g = 0.89$  for  $r = 50 \mu\text{m}$  and increases only to  $g = 0.91$  for  $r = 1000 \mu\text{m}$ , whereas  $\bar{\omega}$  decreases from  $0.995$  to  $0.91$ . (This

is reminiscent of Hansen and Pollack's (1970) finding that "for wavelengths less than  $2.5 \mu\text{m}$  the reflectivity of thick clouds depends primarily on the single-scattering albedo.")

The largest effect of grain size is seen in the near infrared, where the albedo may fall by a factor of 2 or more between  $r = 50 \mu\text{m}$  and  $r = 1000 \mu\text{m}$ . By comparison, the reductions of albedo in the visible are small, never exceeding 10–15%. Thus the fall in spectrally integrated albedo with age, which frequently has been observed in the field, is primarily due to the near infrared. This agrees with satellite observations by Strong *et al.* (1971), who saw little change in the visible channel between dry snow and melting snow, but a dramatic drop in the near-IR reflectance due to melting.

There are peaks in albedo near  $\lambda = 0.4, 1.1, 1.3, 1.85$  and  $2.3 \mu\text{m}$  which correspond to the minima in the absorption coefficient (Fig. 1). Unlike the other peaks, the main one at  $\lambda = 0.4 \mu\text{m}$  becomes more pronounced as the grain size increases.<sup>7</sup> There is also a peak at  $\lambda = 3.1 \mu\text{m}$ , which corresponds to a *maximum* in ice absorption. In this case absorption is so large that the grains have augmented back-reflection (like polished metal spheres). We are not aware of any experimental confirmation of this rather peculiar peak.

At  $\lambda = 2.0 \mu\text{m}$  and  $2.8 \mu\text{m}$  the albedo reaches minimum values of  $0.007$  and  $0.001$  beginning at grain radii of  $500$  and  $100 \mu\text{m}$ , respectively; further increase in size does not further decrease the albedo below these residuals. Between  $\lambda = 3.5 \mu\text{m}$  and  $\lambda = 9 \mu\text{m}$  the residual albedo is  $0.01$ , and it is attained for all grains larger than  $r = 100 \mu\text{m}$ . These residuals are due to the fact that  $\bar{\omega}$  has a lower limit of about  $0.5$  as noted in Section 4b.

Beyond  $\lambda = 5 \mu\text{m}$ , the albedo results (Fig. 4b) are really only of use to calculate the directional emissivity, which follows immediately from

$$\epsilon_s(\mu) = 1 - a_s(\mu) \quad (9)$$

as a consequence of Kirchhoff's law (Siegel and Howell, 1972). Clearly, our model is predicting emissivities of  $\sim 99\%$  in this case, in agreement with observations of Griggs (1968), although there is a significant zenith angle dependence which we shall

<sup>7</sup> Some investigators find the main peak in spectral albedo to be at larger wavelengths than  $0.4 \mu\text{m}$ . In our calculation, this peak corresponds to the minimum in the measured absorption coefficient of ice. Assuming that our source (Sauberer, 1950) used an 18 cm block of ice, his measured transmittances were 99.3, 99.1 and 98.5% at  $\lambda = 0.40, 0.45$  and  $0.50 \mu\text{m}$ , respectively. A very slight error in Sauberer's measurements could shift the calculated albedo maximum. But the deep blue color in glacial crevasses indicates the peak cannot be at a wavelength far from  $0.4 \mu\text{m}$ . The observations of peaks at larger wavelengths are probably due to dust in the snow (see Fig. 5 of Part II).

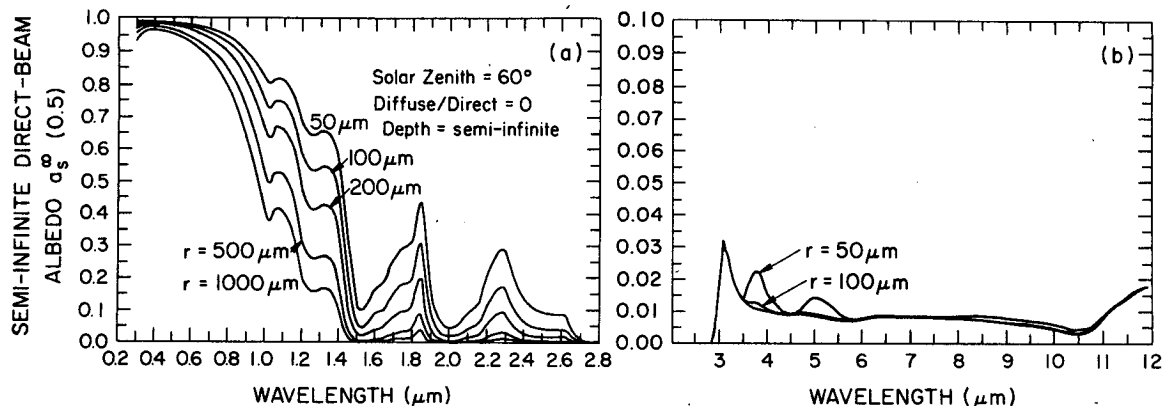


FIG. 8. Semi-infinite direct beam albedo  $a_s^\infty(0.5)$  as a function of wavelength for various grain radii.

see later. The emissivity exhibits very little dependence on grain size.

Bohren and Barkstrom (1974), by assuming a single-scattering albedo close to unity (valid for the visible part of the spectrum), derived a simplified relation between semi-infinite diffuse albedo and grain size [their Eq. (42)]

$$1 - a_d^\infty \propto r^{1/2}. \tag{10}$$

This square-root dependence on grain size was also found by Giddings and LaChapelle (1961, their Eq. 21). To determine the extent of its validity, we have plotted  $a_d^\infty$  in Fig. 9 versus the square root of the grain radius for several wavelengths. We see that the relation (10) holds for the visible wavelengths 0.4 and 0.8  $\mu\text{m}$  but not for longer wavelengths. This breakdown in (10) occurs whenever  $\omega$  drops below 0.99, i.e., beyond about  $\lambda = 0.9 \mu\text{m}$ .

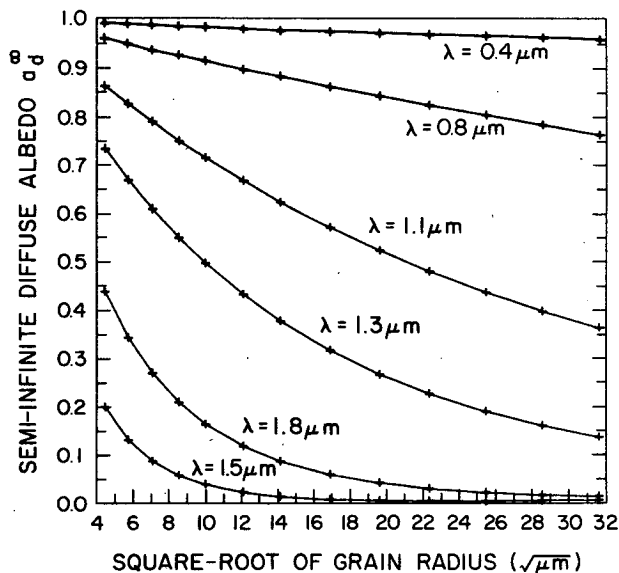


FIG. 9. Diffuse albedo  $a_d$  versus square root of grain radius for seven discrete wavelengths.

*b. Effect of liquid water content*

Field experience indicates that snow albedo decreases as the liquid water content increases (e.g., Grenfell and Maykut, 1977). We can speculate about the reason for this. Liquid water replaces air between ice grains (Colbeck, 1975; 1979). The spectral refractive index of liquid water is very close to that of ice for  $\lambda < 5 \mu\text{m}$  (Irvine and Pollack, 1968, Figs. 1, 2). The replacement of air by liquid water between ice grains can thus increase the effective grain size. (This argument does not apply to the microwave part of the electromagnetic spectrum. There  $m_{\text{ice}}$  and  $m_{\text{water}}$  differ considerably, leading to dramatic differences in microwave emissivity between wet and dry snow.)

There is some observational evidence for this view that the liquid water reduces snow albedo only by increasing the effective grain size. We reproduce here (Fig. 10) a figure from O'Brien and Munis (1975, their Fig. 9).<sup>4</sup> They observed the spectral albedo of a snow sample to be lower after warm air

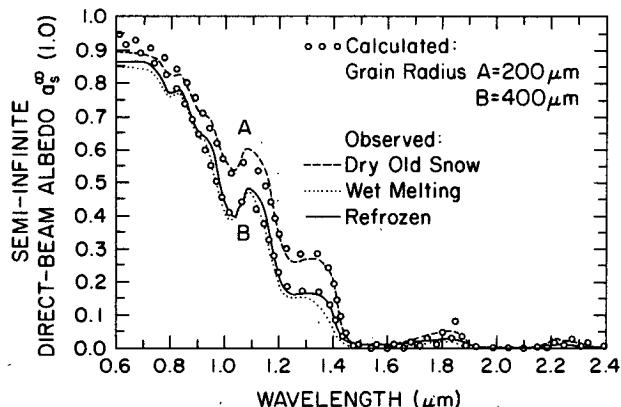


FIG. 10. Comparison of calculated spectral albedo with laboratory measurement of snow reflectance; effect of liquid water content. Observations are taken from O'Brien and Munis (1975)<sup>4</sup> but corrected by us for the reflectance of the BaSO<sub>4</sub> standard they used.

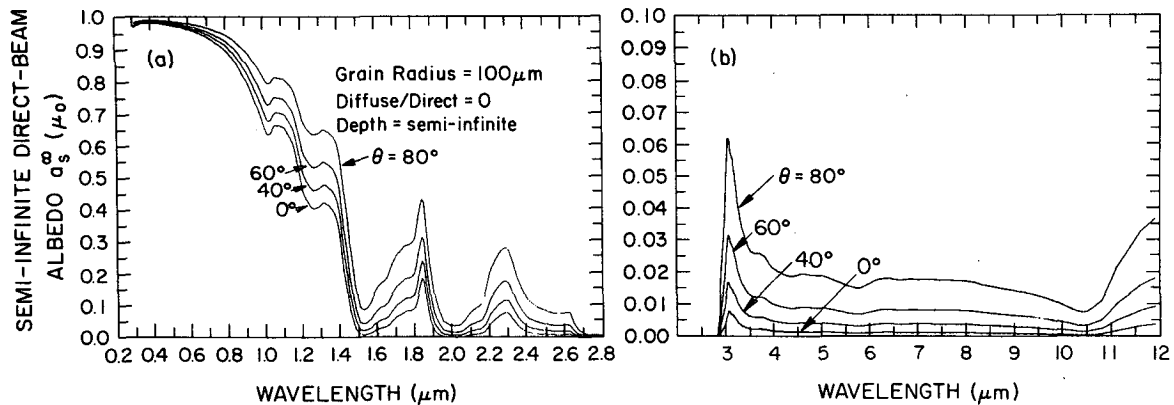


FIG. 11. Semi-infinite direct-beam albedo  $a_s^\infty(\mu_0)$  versus wavelength for several values of direct-beam zenith angle  $\theta = \cos^{-1}\mu_0$ .

had been blown over it so that the surface was wet. But there was no further change in albedo when the sample was refrozen. There was then no liquid water present, but the water bridges between grains had presumably frozen, with no change in the effective grain size.

In addition to changing the effective grain size by its mere presence, liquid water also speeds up the rate of grain growth. This explains why only a short exposure to melting conditions can reduce the albedo considerably.

### c. Dependence on solar zenith angle

In Section 4c we plotted a number of observations of the sun-angle dependence of snow albedo and saw that they were not inconsistent with our model predictions. But those predictions were not spectrally-integrated whereas some of the observations were. Also, many instruments do not exhibit a proper "cosine-law" response at large zenith angles (Dirn-hirn and Eaton, 1975), which leads them to consistently overestimate the albedo at such zenith angles. Another cause of increase in albedo with zenith angle which we have not considered in our model is specular reflection at glancing incidence from a thin ice layer ("firnspiegel") which is sometimes present. Middleton and Mungall's (1952) measurements indicate a definite specular reflection developing near grazing incidence for glazed crust. This may account for observations (e.g., Hubley, 1955) showing that, in early morning when an ice crust is sometimes present due to nighttime refreezing of meltwater, the albedo is higher than at the same solar zenith angle in late afternoon. Thus, while we consider that our model furnishes useful predictions of the sun-angle dependence, we realize that neither they nor the measurements are definitive.

Fig. 11 shows our calculated spectral albedo  $a_s^\infty(\mu_0)$  for direct solar radiation at zenith angles

from 0 to 80°. The albedo increases at all wavelengths as the zenith angle increases. Relative to direct overhead sun, the albedo increases only a few percent in the visible but by as much as 0.2 in the near-IR. It is clear that albedo changes most rapidly with  $\theta_0$  at large values of  $\theta_0$ . This is because  $\theta_0$  enters our equations only as  $\mu_0 = \cos\theta_0$ , which changes slowly for small  $\theta_0$ . This explains Petzold's (1977) empirical rule-of-thumb that snow albedo is virtually independent of  $\theta_0$  for  $\theta_0 < 50^\circ$ .

Our calculations are for a flat snow surface. Because of suncups on temperate glaciers (e.g., Post and LaChapelle, 1971, Figs. 85–88), sastrugi on polar glaciers, and other surface features, the effective zenith angle probably rarely reaches 80°. The nonplanarity of the snow surface will play a much greater role at grazing incidence. Surface elements with a larger  $\mu_0$  than the planar value will tend to contribute more to the average or effective value of  $\mu_0$  than those with  $\mu_0$  less than the planar value, because the latter will more often be in shadow and so contribute nothing. Hence the average  $\mu_0$  will be smaller than the planar value. [In the South Polar region, fields of oriented sastrugi ridges can cause a local diurnal cycle of albedo of ~3% even though the solar zenith angle is constant throughout the day (M. Kuhn, personal communication).] Furthermore, as the sun goes to very high zenith angles, the incident radiation becomes dominated by sky radiation rather than direct radiation, so the effective zenith angle becomes less than the solar zenith angle. This should lead to a peak in the albedo as a function of  $\theta_0$  rather than a simple monotonic increase all the way to  $\theta_0 = 90^\circ$ .

In Fig. 11b we have continued the albedo calculation out to  $\lambda = 12 \mu\text{m}$ , to show the albedo peak at  $3.1 \mu\text{m}$  discussed earlier and also the behavior of directional snow emissivity  $\epsilon_s(\mu)$  [Eq. (9)]. In the atmospheric window region ( $8 \leq \lambda \leq 12 \mu\text{m}$ ), we see that a decrease of emissivity toward grazing

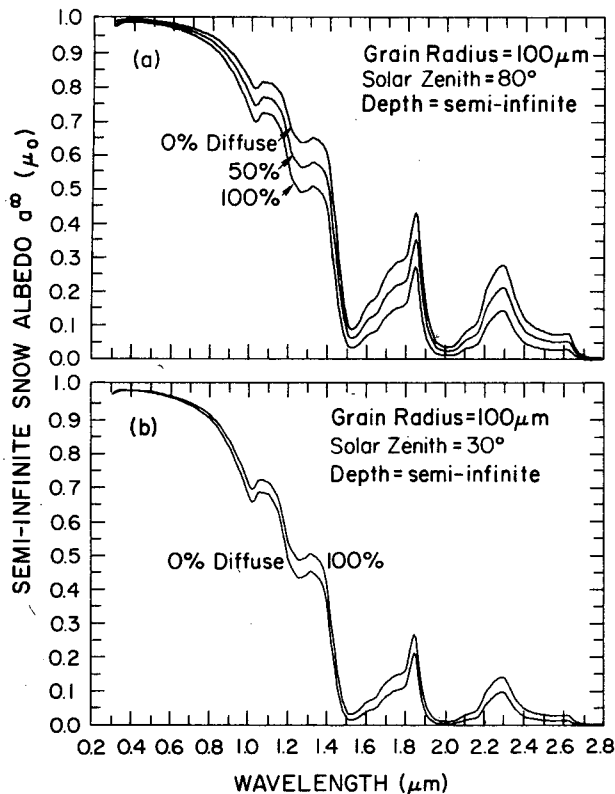


FIG. 12. Semi-infinite net albedo  $a_{net}^{\infty}$ , versus wavelength for various ratios of diffuse to direct radiation.

angles is predicted. For example, at  $\lambda = 12 \mu\text{m}$ ,  $\epsilon_s = 0.963$  for  $\theta_0 = 80^\circ$  increasing to 0.996 for  $\theta_0 = 0^\circ$ . Also, the emissivity decreases steeply between 10.5 and 12  $\mu\text{m}$ . Remote sensing over snow in the infrared window region may have to account for such nonunit emissivities and their spectral and angular variation.

#### d. Effects of cloud cover

Cloud cover influences snow *spectral* albedo by converting direct radiation into diffuse radiation and thus changing the effective zenith angle. Eq. (8) allows the calculation of albedo for any given ratio of diffuse to direct incidence. Fig. 12 shows some results from this equation. In Fig. 12a we see that when  $\theta_0 = 80^\circ$ , the albedo is *reduced* when the diffuse fraction is increased. This is because the purely diffuse radiation has an effective zenith angle near  $50^\circ$ ; thus, converting direct into diffuse radiation reduces the effective zenith angle, thereby reducing the albedo.

When the sun is high the effect of cloud cover is just the opposite. Fig. 12b shows that for  $\theta_0 = 30^\circ$  conversion of direct into diffuse radiation slightly increases the albedo. Near  $\theta_0 = 50^\circ$  the formation of cloud cover would leave spectral snow albedo virtually unaltered.

For the *spectrally integrated* albedo, one must also consider that clouds change the spectral composition of the radiation incident on the snow. They cause the radiation field to become relatively richer in visible wavelengths. This tends to increase the snow albedo, which acts counter to the zenith angle effect for  $\theta_0 > 50^\circ$  (typical of snow-covered regions). That the visible-enrichment effect almost always wins out is indicated by numerous observations (e.g., Liljequist, 1956). But that the zenith-angle effect is operative is indicated in Rusin's (1961, Table 173) Antarctic measurements; he found the spectrally-integrated albedo to increase only from 0.83 (clear) to 0.90 (overcast) at  $\theta_0 = 80^\circ$ , while it increased all the way from 0.74 to 0.93 when  $\theta_0 = 45^\circ$ .

#### e. Dependence on snowpack thickness

The albedo of a thin snowpack obviously depends upon the albedo of the underlying surface; only when the snowpack becomes thick enough are the effects of the underlying surface obliterated. Here we shall examine just how thick a snowpack must be before it can be regarded as "effectively semi-infinite."

Eq. (1) indicates that, because of the inverse dependence of optical depth on grain radius  $r$ , radiation will penetrate deeper into a pack of larger particles if the density  $\rho$  is kept fixed. This can be seen immediately in Fig. 13, which shows calculated spectral albedo for various snowpack thicknesses (given in liquid water equivalent) with a black underlying surface. Beyond  $\lambda = 2.8 \mu\text{m}$  less than 1 mm is required to make the pack optically semi-infinite, and indeed beyond about  $\lambda = 1 \mu\text{m}$  it seems unlikely that the effect of finite thickness will ever be seen. The thin-snowpack albedos differ substantially from the semi-infinite case only in the visible region where the radiation penetrates to much greater depths than in the near infrared.

The liquid-equivalent depth for which the snowpack becomes effectively semi-infinite (i.e., albedo at all wavelengths within 1% of that for an infinitely-thick snowpack) is 2 cm for grain radius  $r = 50 \mu\text{m}$  (e.g., 20 cm of fluffy new snow,  $\rho = 0.1 \text{ g cm}^{-3}$ ), about 8 cm for  $r = 200 \mu\text{m}$  (e.g., 20 cm of fine-grained old snow,  $\rho = 0.4$ ) and 20 cm for  $r = 1000 \mu\text{m}$  (e.g., 50 cm of old melting snow of  $\rho = 0.4$ ). This means that as a snowpack of less than 20 cm liquid equivalent ages and the grain size increases, so that the pack's optical thickness decreases, one may eventually "see" the ground through it even in the absence of melting and runoff. Thus, two snowpacks, one of which becomes optically finite as grain size increases while the other does not, will show differing albedo time series even if their grain size time series are identical.

Our results as to what constitutes semi-infinite snow are in general agreement with some other investigators. Schlatter (1972), based on an examination of Antarctic snow measurements, indicates at least  $d = 50$  cm is necessary. Bergen (1975) indicates a figure of  $d = 30$  cm, while Grenfell (1979) indicates  $d = 10$ – $20$  cm. These investigators were considering snows which differed greatly in density and grain size, and an examination of Fig. 13 shows how they could come up with differing numbers.

However, our calculations fail to explain the dependence of albedo on depth found by Giddings and LaChapelle (1961, Fig. 2). For  $\lambda = 0.59 \mu\text{m}$  and  $r = 250 \mu\text{m}$ , their measured albedo rose rapidly as thickness increased to 2 cm. At 2 cm the albedo was within 3% of the asymptotic limit. In Fig. 13b our calculations are for grains near this size ( $r = 200 \mu\text{m}$ ) and at  $\lambda = 0.59 \mu\text{m}$  we appear to need 3 cm of liquid-equivalent depth to obtain an albedo within 3% of the asymptotic limit. For a density we guess to be 0.4, this is a geometric depth of 7.5 cm, i.e., 4 times as deep as the experiment showed. This discrepancy is addressed in Part II (Warren and Wiscombe, 1980).

An interesting effect of finite depth is that it considerably flattens the spectral albedo curves between  $\lambda = 0.3 \mu\text{m}$  and  $\lambda = 0.8$ – $0.9 \mu\text{m}$ . This may explain several observations (see Mellor, 1977) showing very flat spectral snow albedos.

#### f. Effect of snow density on albedo

Some investigators find snow albedo to be a function of snow density (e.g., Arai, 1966; Bergen, 1975). O'Brien and Munis (1975)<sup>4</sup> also noticed that an increase in density correlated with a decrease of albedo, but they cautioned that density was often correlated with other symptoms of aging, such as grain size, and were skeptical as to whether density per se influenced albedo.

Our calculated albedo does not depend upon density. One would expect this to be true as long as curves like those of Mellor (1977) for flux extinction coefficient are about linear in density, which is true up to densities of  $\sim 0.4 \text{ g cm}^{-3}$ . Beyond that density, shadowing of grains and other near-field phenomena could introduce a dependence of albedo on density. This matter is discussed further in Section 7.

Bohren and Barkstrom's (1974) formula for snow albedo also does not involve the density, and Bohren and Beschta (1979) have done a relevant experiment. They measured spectrally integrated albedo ( $0.35$ – $2.8 \mu\text{m}$ ) of a snowpack immediately before and after running a snowmobile over it. The compaction by the snowmobile increased the density, from  $0.05$  to  $0.20 \text{ g cm}^{-3}$  or from  $0.30$  to  $0.45 \text{ g cm}^{-3}$ , but there was insufficient time between measure-

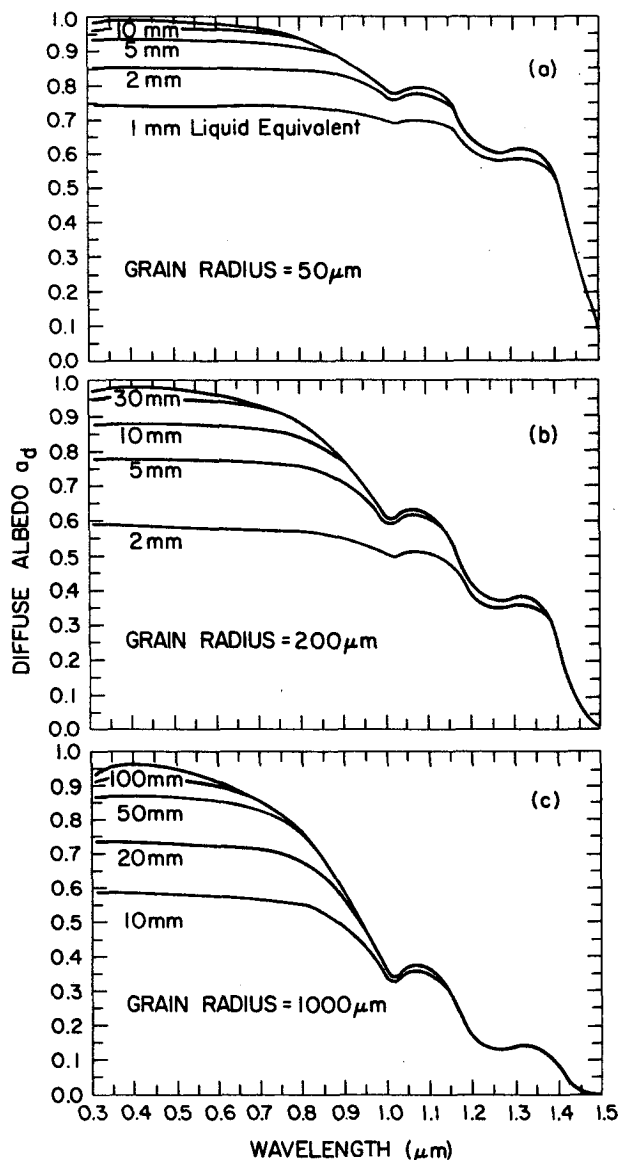


FIG. 13. Direct beam albedo  $a_s^0(\mu_0)$  versus wavelength for various grain radii; and, for each grain radius, for a variety of snow depths expressed in liquid equivalent. The top curve in each case is for semi-infinite depth.

ments for the grain size to change, and the change in albedo was insignificant.

#### g. Sensitivity of albedo calculation to error in absorption coefficient

We pointed out in Section 4a that in some spectral regions different values of ice imaginary refractive index  $m_{\text{im}}$  have been obtained by different investigators. Fig. 14 shows the spectral albedo calculated for our standard snowpack, with  $m_{\text{im}}$  everywhere multiplied by 0.5, 1, 2, 5 or 10 for all  $\lambda \leq 2.0 \mu\text{m}$ . (For  $\lambda > 2.0 \mu\text{m}$  we think there is little uncertainty.)

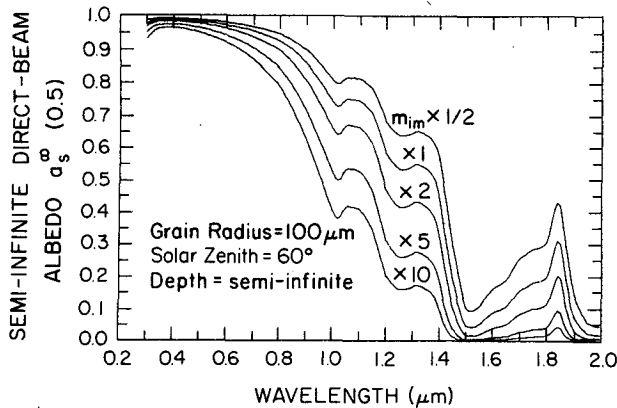


FIG. 14. Sensitivity of spectral albedo calculation to error in absorption coefficient of ice.

For  $0.33 \leq \lambda \leq 0.45 \mu\text{m}$ , Kalitin's (1936) values for  $m_{im}$  are about 10 times as large as Sauberer's (1950), which we used. This difference is seen to reduce the albedo by only 2–3%. For longer wavelengths the sensitivity of albedo to error in  $m_{im}$  becomes more pronounced, but the uncertainty in  $m_{im}$  is less beyond about  $\lambda = 1 \mu\text{m}$  (typically no more than a factor of 2). It can be seen that the strange "finger" in the albedo curve near  $\lambda = 1.85 \mu\text{m}$ , which as we discussed earlier is not observed, would be eliminated if  $m_{im}$  would be multiplied by factors ranging from 1 to 2 in the region  $1.80 \leq \lambda \leq 1.86 \mu\text{m}$ .

## 6. Comparison of calculations with observations of snow reflectance

### a. Near-infrared

O'Brien and Munis (1975)<sup>4</sup> made laboratory measurements of the bidirectional spectral reflectance of natural snow. Their measurements were relative to a  $\text{BaSO}_4$  standard, so we took their raw values and corrected them for the diffuse reflectance of  $\text{BaSO}_4$  (Grum and Luckey, 1968). Their snow thicknesses were always in the range 10–20 cm, which is sufficiently thick that the albedo is within 1% of that of a semi-infinite snowpack, as we showed in Section 5e, except possibly for old melting snow. Figs. 10 and 15 are typical of their results, which were for a source zenith angle of  $0^\circ$  and detector zenith angle of  $30^\circ$ .

Curve A of Fig. 15 was from a sample of fresh snow, and Curve B from a sample of the same snowfall after two days of natural aging at temperatures hovering above and below freezing. We are able to fit these curves with our albedo function  $a_s(1)$  (dashed lines) for  $r = 50 \mu\text{m}$  and  $r = 200 \mu\text{m}$  although there are significant disagreements. The calculated albedo falls below the reflectance measurements for  $\lambda < 1.2 \mu\text{m}$ . The calculated peak at

$1.1 \mu\text{m}$  is not sharp enough. The peak at  $\lambda = 2.3 \mu\text{m}$  is shifted to higher wavelength relative to the observation. And at  $\lambda = 1.85 \mu\text{m}$  there is a spike in the calculated albedo which does not appear in the measurements, although we have given what we think is the correct explanation of this problem in Section 5g.

At the other wavelengths, there are several factors which may be contributing to the disagreements we see:

- 1) Our calculated albedo  $a_s^\infty(\mu_0 = 1)$  corresponds to the *integral* of O'Brien and Munis's bidirectional reflectance over all detector angles (weighted by cosine of detector angle). They tried different source and detector angles, although only out to  $30^\circ$  at most; the variability they found with detector angle is large enough and in the right direction to explain most of the disagreements, especially for  $\lambda < 1.2 \mu\text{m}$ . We might note that spectrally detailed near-infrared reflectance measurements over snow are rare indeed; thus, while it is less than desirable to compare directional albedo with bidirectional reflectance, the comparison at least validates the performance of the model in a broad sense.

- 2) Experimental error is estimated to be  $\sim 5\%$  by O'Brien and Munis, but it grows worse as one approaches the visible, as indicated by the unrealistic erratic oscillations in their curves starting at  $\lambda = 0.75 \mu\text{m}$ .

- 3) Values of ice absorption are still uncertain by up to 20–50% at some near-IR wavelengths. However, as can be seen in Fig. 14, it would take a factor of 2 decrease in ice imaginary index at  $0.6 \leq \lambda \leq 1.2 \mu\text{m}$  to bring calculation into agreement with observation, and this seems unrealistic.

- 4) The factor for conversion from reflectance relative to  $\text{BaSO}_4$  powder to true reflectance is still not entirely agreed upon for  $0.3 \leq \lambda \leq 0.7 \mu\text{m}$  (Patterson *et al.*, 1977). But the disagreement is at

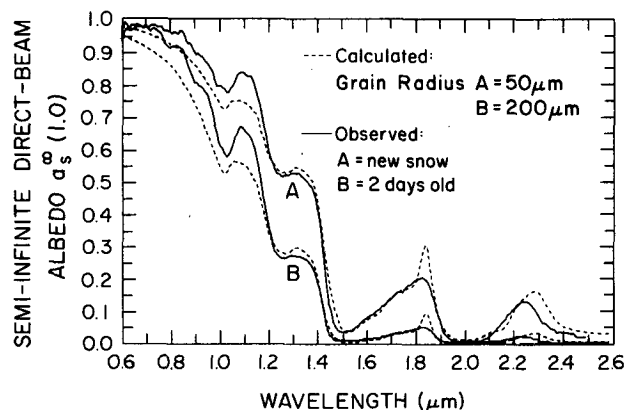


FIG. 15. Comparison of calculated spectral albedo with O'Brien and Munis laboratory observations of snow reflectance.

the 3% level. The reflectance of O'Brien and Munis's BaSO<sub>4</sub> standard would have to differ by up to 10% from accepted values to explain completely the discrepancies in Fig. 15.

However, the size (and even the sign) of the discrepancy between our calculation and O'Brien and Munis's observation is different for different snow samples. Fig. 10 shows results for a snow sample that was taken through a melting and re-freezing cycle compared to our calculated  $a_s^\infty(1)$  for  $r = 200$  and  $400 \mu\text{m}$ , which gives the best fit for  $\lambda \geq 1.2 \mu\text{m}$ . Here our calculation *overestimates* the measurements for  $\lambda \leq 0.85 \mu\text{m}$  by up to 0.05. This suggests that reasons (1) and (2) above are the major contributors to the discrepancies. However, in both Figs. 10 and 15 our calculation is seen to underestimate the peak at  $\lambda = 1.1 \mu\text{m}$ . This is possibly due to an error in the measured  $m_{\text{im}}$  of ice.  $m_{\text{im}}$  for liquid water is about a factor of 2 lower at its local minimum here. Fig. 14 shows that a factor of 2 error would be the right size to explain this discrepancy.

Overall, it may be said that our model furnishes a respectable simulation of near-infrared spectral snow albedo. It is capable of matching a large number of data points by adjusting but a single parameter—the effective grain size. Furthermore, the values of grain size selected are entirely in concord with the known range of grain sizes for fresh, middle-aged and old snow (see Section 3b).

*b. Visible*

Fig. 16, which we have reproduced from Mellor's (1977) review article, summarizes some field measurements of spectral snow albedo in the visible. They obviously agree neither in magnitude nor trend. The measurements of Thomas, which increase monotonically, particularly lack credibility. Those of Krinov were made in the 1930's in Russia with

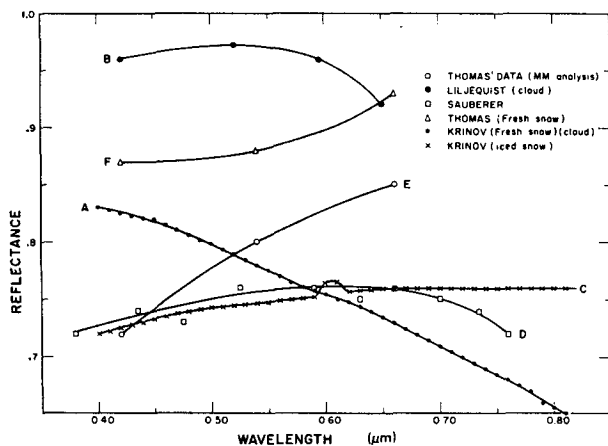


FIG. 16. Reflectance of snow as a function of wavelength in the visible, according to various investigators. From Mellor (1977).

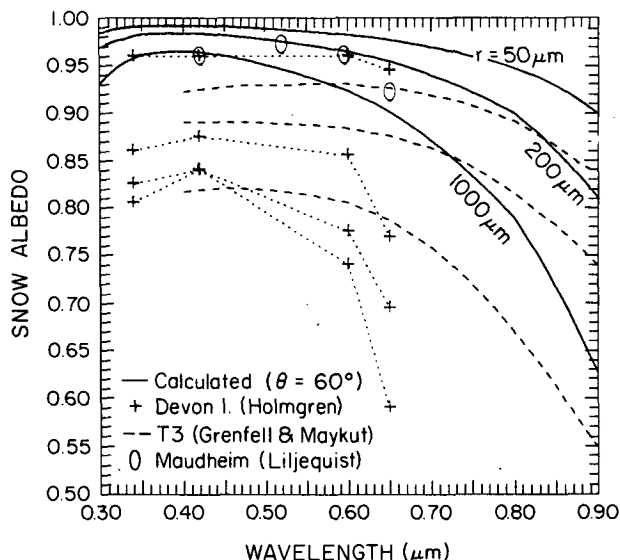


FIG. 17. Spectral albedo of snow in the visible, comparisons of calculation with observations.

instruments of uncertain accuracy. Rarely was grain size, or even the age or state of the snow surface, specified very well if at all. This goes also for many measurements not shown in Fig. 16.

For comparison with our calculations, we have selected some observations made with good instruments under well-defined conditions, which are plotted in Fig. 17. Liljequist (1956) measured snow albedos at four visible wavelengths at Maudheim, on a small ice shelf at the coast of Antarctica, during the period 1949–52. He made his observations under overcast conditions so that errors could not be introduced by possible lack of a cosine-law response in his instrument. The albedos for this dry fine-grained snow were among the higher ever obtained, dropping from 97% at  $\lambda = 0.52 \mu\text{m}$  to 92% at  $\lambda = 0.65 \mu\text{m}$ . These reported values are averages of measurements made on five different days for different snow conditions. (The range between high and low values at each wavelength was 0.6–2.3%.) Holmgren (1971) measured albedos at four visible wavelengths at Devon Island in the Canadian Archipelago (75°N) in summer 1962. In order of decreasing albedo, the four curves are (a) new loose snow on top of hard wind-packed snow, (b) frozen snow over wet melting snow, (c) melting well-drained snow and (d) melting soaked snow. Grenfell and Maykut's (1977) observations are for snow at Ice-Island T3 in the Arctic Ocean. In order of decreasing albedo, they are dry cold snow, wet new snow and melting old snow. They used the portable spectrophotometer designed by Roulet *et al.* (1974). Its spectral resolution was good, being at worst  $\sim 0.2 \mu\text{m}$  (at  $\lambda = 0.9 \mu\text{m}$ ).

The calculated albedos (solid lines) are for  $r = 50$ , 200 and 1000  $\mu\text{m}$ , respectively. They are taken from Fig. 8. The calculation was for direct incidence at  $\theta = 60^\circ$ , but the curves would be insignificantly different for diffuse incidence. The calculated albedos for new snow ( $r = 50 \mu\text{m}$ ) exceed those measured by Holmgren and Liljequist by 2–6%. They disagree even more with the top curve of Grenfell and Maykut, but these measurements were for “wind-packed” snow, not necessarily new, of undetermined grain size. While the discrepancy between observation and calculation for *new* snow might possibly be explained by observational error, this cannot be said for old and melting snow. The model is clearly calculating unreasonably high albedo values for old and melting snow. This failure of the model in the visible region is in clear contrast to its success in the near-IR, where the decrease in albedo with aging was seen to be adequately described by the increase in grain size in the model. The value of  $m_{\text{im}}$  is so small in the visible that an increase in grain radius to 1 mm fails to reduce the albedo (at  $\lambda = 0.4 \mu\text{m}$ ) below 96%. Snow grains are rarely larger than  $r = 1 \text{ mm}$ , but even the use of an unreasonably large grain size ( $r = 4 \text{ mm}$ ) fails to reduce the calculated albedo (at  $\lambda = 0.4 \mu\text{m}$ ) below 92%.

There are several possible explanations for the discrepancies:

- 1) The effects of nonsphericity and/or close packing of snow crystals can be ignored in the near-infrared where  $m_{\text{im}}$  is large but become important when  $m_{\text{im}}$  is small. This possibility is discussed in Section 7.

- 2) Our values of  $m_{\text{im}}$  in the visible may be too small. But they would have to be 3–40 times larger (40 at  $\lambda = 0.4 \mu\text{m}$ , smaller factors for larger  $\lambda$ ) to mimic the observations. Kalitin (1936) indeed reported values of  $m_{\text{im}}$  6–10 times larger than ours (Sauberer, 1950) in the spectral range  $0.33 \leq \lambda \leq 0.45 \mu\text{m}$ , but all in all we think Sauberer’s values are more reliable. If anything, Sauberer’s values should be too *large*, because he used lake ice rather than pure ice. Furthermore, the  $m_{\text{im}}$  of liquid water, which is more easily measured than that of ice, also reaches such low values as  $7 \times 10^{-10}$  (Patel and Tam, 1979; Tam and Patel, 1979). This is a factor of 2 *smaller* than our minimum  $m_{\text{im}}$  for ice. Since at longer wavelengths the  $m_{\text{im}}$  of ice and water do not differ by more than a factor of 6, and this only because of shifts in band positions (Irvine and Pollack, 1968), it seems unlikely that they could differ by a factor of 40 at  $\lambda \approx 0.4 \mu\text{m}$ . Still, we would suggest a careful remeasurement of  $m_{\text{im}}$  in the visible as a high-priority task.

- 3) We also considered whether the snow used for the measurements in Fig. 17 was effectively semi-

infinite. Finite depth would provide just the effect we see: a reduced albedo in the visible but no change in the near-IR (Fig. 13). But it turns out that for only one of the curves in Fig. 17 can the low albedo be partly due to insufficient depth. This is the middle curve of Grenfell and Maykut (1977) which was for  $\sim 2 \text{ cm}$  (liquid equivalent) of snow on top of white ice; we examine this situation in detail in Part II. Their other two samples were thick snow-packs, and the samples of Liljequist (1956) and Holmgren (1971) were certainly semi-infinite, being an ice shelf and a glacier, respectively.

- 4) The remaining possibility is that the small amounts of absorptive impurities present in natural snow can effectively reduce the visible albedo. [Dunkle and Bevans (1956) and Giddings and LaChapelle (1961) both mention this effect as a possibility but they present no estimates or calculations of it, and in fact Giddings and LaChapelle dismiss it as unimportant.] The effect of impurities is examined in Part II (Warren and Wiscombe, 1980).

## 7. Effects of close packing and nonsphericity

### a. Close packing

The Mie scattering calculations are for a plane electromagnetic wave incident on a single isolated sphere of ice. Spheres in an assemblage will retain the single-scattering properties ( $\bar{\omega}, g, Q_{\text{ext}}$ ) that they would have in isolation, provided that they are not in a regular array, and that they are not in each other’s “near field.” They must be sufficiently far apart that 1) interparticle interference effects are negligible; 2) each grain is exposed to an incident plane wave; and 3) grains do not shadow one another. Cloud droplets, for example, would be sufficiently far apart that near-field effects would not appear. In a snowpack the individual grains are not in a regular array, but they are close together, so we must fact the possibility that our Mie calculations do not correctly give the single-scattering properties. Specifically, we want to know whether our model’s failure to match observations of visible snow albedo is due to its neglect of near-field effects.

It should be noted that the far-field assumption is made only in that part of our model using Mie theory. The  $\delta$ -Eddington approximation for multiple scattering (as well as other radiative transfer methods, such as the diffusion approximation used by Giddings and LaChapelle, 1961) should be applicable to radiative transfer in a close-packed medium, as long as it is provided with appropriate single-scattering quantities.

#### 1) INTERPARTICLE INTERFERENCE

The breakdown of the far-field approximation as the density increases has been documented experi-

mentally for closely packed particles with size parameter  $x \approx \lambda$ . Blevin and Brown (1961) studied suspensions of submicron-diameter pigment particles in water or air. The reflectance at visible wavelengths ( $0.4 \leq \lambda \leq 0.7 \mu\text{m}$ ) for an optically semi-infinite suspension of  $\text{MgCO}_3$  particles in air was found to be independent of density up to a volume concentration of 30%, but to decrease with further increase in volume concentration. This is what one might expect for these small particles: as the density increases, the interparticle separation is reduced to the order of a wavelength, so adjacent particles scatter more and more coherently. The scattering behavior of two adjacent particles may approach that of a single larger particle (Vedernikova and Kabanov, 1974), reducing  $\tilde{\omega}$  and/or increasing  $g$ , both of which would reduce the albedo.

A simple device (Heller, 1945; Hiltner and Krieger, 1969) which has been used to correct Mie calculations for this near-field effect is to replace the refractive index of the surrounding medium by a volume-weighted average of the refractive indices of the medium and the suspended particles. Gate (1973) measured the volume scattering coefficient of dense suspensions of polystyrene spheres in water as a function of volume concentration, wavelength (visible), and particle size. He obtained good agreement with almost all of his experimental data by taking the effective refractive index of the surrounding medium not as that of pure water but rather as

$$m_{re}^{med} = (1 - v)m_{re}^w + vm_{re}^s, \quad (11)$$

where

- $v$  volume-fraction of spheres
- $m_{re}^s$  real refractive index of spheres
- $m_{re}^w$  real refractive index of water.

Then for his Mie calculations he used

$$\left. \begin{aligned} m_{re} &= m_{re}^s / m_{re}^{med} \\ x &= 2\pi r m_{re} / \lambda \end{aligned} \right\}, \quad (12)$$

where  $\lambda$  is the wavelength in vacuum.

The results of employing such an adjusted  $m_{re}$  in our model for snow were that  $Q_{ext}$  and  $\tilde{\omega}$  both decreased insignificantly, but  $g$  increased considerably.

The insensitivity of  $\tilde{\omega}$  to the presence of nearby spheres seems plausible from a geometrical optics viewpoint.  $(1 - \tilde{\omega})$  is the ratio  $Q_{abs}/Q_{ext}$ .  $Q_{abs}$  is determined almost entirely by rays passing through the sphere (as opposed to edge rays or diffracted rays), and these are not much influenced by nearby spheres, as follows from the very definition of a ray (see Born and Wolf, 1965, Chap. III).  $Q_{ext}$ , which is near 2 for large ice grains in the far-field, might be reduced if close-packing caused diffraction to be reduced, as suggested by Sarofim *et al.* (1968).

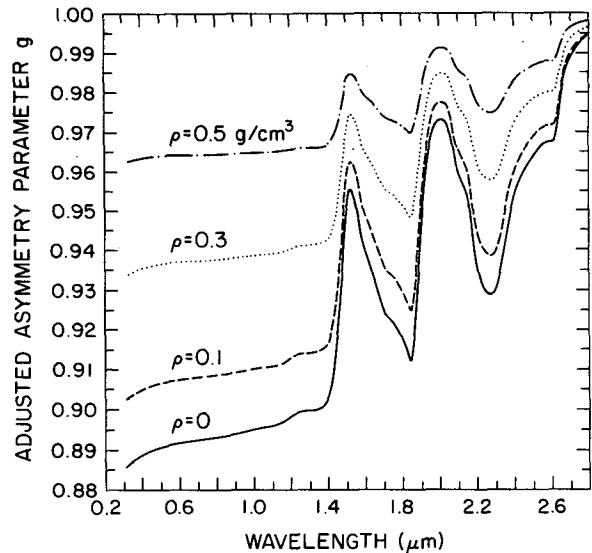


FIG. 18. Near-field test; effect on asymmetry parameter of adjusting the refractive index of the surrounding medium (air) using Eq. (11).

But even if diffraction were to disappear completely,  $Q_{ext}$  would approach 1 and thus  $(1 - \tilde{\omega})$  would be increased only by a factor of 2, not the factor of 50–100 which we would need to reduce calculated visible albedo to observed values. (From Figs. 3 and 8 it can be seen that at  $\lambda = 0.4 \mu\text{m}$ , an increase in  $(1 - \tilde{\omega})$  by a factor of 20 reduces the albedo by only 3%.) This relative insensitivity of  $\tilde{\omega}$  to  $m_{re}$  is also in concert with an approximation of Sagan and Pollack (1967), which comes from the lowest order truncation of the geometrical optics formula, showing that  $\tilde{\omega}$  is a function only of  $m_{im}$ .

For the asymmetry factor  $g$ , Fig. 18 shows the results of Mie calculations using the adjusted  $m_{re}$  of (11) and (12), for snow ( $r = 200 \mu\text{m}$ ) of density  $0 \leq \rho \leq 0.5 \text{ g cm}^{-3}$ . For all wavelengths the scattering becomes more forward-directed. In the visible,  $g$  increases from 0.89 in the far-field limit to 0.96 for  $\rho = 0.5$  (near the upper limit for the density of a surface snow layer).

Since the major effect of this adjustment in  $m_{re}^{med}$  was to increase  $g$ , we calculated snow albedo for  $r = 200 \mu\text{m}$  (Fig. 19) using specified values of  $g$  higher than that calculated for the far-field limit. Raising  $g$  to a uniform value of 0.96 for  $0.3 \leq \lambda \leq 1.5 \mu\text{m}$  decreases the albedo considerably in the near-IR but only by 1–2% at  $\lambda = 0.4 \mu\text{m}$ . Even when we use a ridiculously large asymmetry parameter ( $g = 0.99$ ) the reduction in albedo at  $\lambda = 0.4 \mu\text{m}$  is only 4%.

This possible near-field effect, therefore, is dramatically inadequate to explain our discrepancy with observations of visible albedo. Furthermore, to agree with observations, we require our calculated

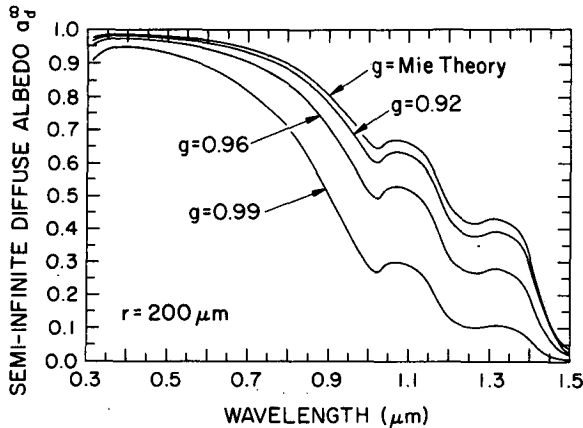


FIG. 19. Effect on snow albedo of artificially raising asymmetry parameter  $g$ .

albedo to be reduced only in the visible, not in the near-IR. This form of a near-field correction does just the opposite and, in fact, up to  $\rho = 0.5$  has an effect similar to that of increasing the grain size in our model (Fig. 8), so if this near-field effect is operative in snow we could probably mimic observations simply by increasing the grain size. This could account for the fact that in Fig. 7 of Part II we require a grain size  $r = 1300 \mu\text{m}$  to match Grenfell and Maykut's (1977) albedo measurement at  $\lambda = 0.9 \mu\text{m}$  for old melting snow, whereas they measured the grain size to be smaller,  $r = 500 \mu\text{m}$ .

However, there is reason to think that interparticle interference is insignificant for shortwave radiation in a snowpack. The experiments of Blevin and Brown (1961) and Gate (1973), as well as other experiments on pigments, paints and polystyrene spheres which showed a dependence of albedo on density (e.g., Harding *et al.*, 1960; Hottel *et al.*, 1971) all involved particles of size  $r$  close to the wavelength  $\lambda$ . At high density the interparticle separation  $\delta$  is also close to the wavelength ( $r \approx \delta \approx \lambda$ ). The interparticle separation between grains in a snowpack, although small relative to the radius  $r$ , would still be large relative to the wavelength ( $r \approx \delta \gg \lambda$ ), so they would not be likely to scatter coherently.

## 2) NONPLANE WAVE

A particle in the near field of another particle is not irradiated by a plane electromagnetic wave. The path lengths and directions of photons passing through a particle in the near field of another will be different than in the far-field case. This will alter  $g$  and  $\bar{\omega}$ , but not by nearly enough to resolve our visible albedo problem. We saw above (Fig. 19) that even an unreasonably large  $g$  had little effect on the visible albedo.  $(1 - \bar{\omega})$  would be increased in the same proportion that the average photon path

length through the particle was increased. (The absorption coefficient in the visible is so small that absorption is nearly linear in path length.) It is difficult to imagine that the difference in average photon path length due to an impinging non-plane wave could be as much as a factor of 2, but we would need even a much greater factor (50–100) to bring the calculated albedo down to the values observed. This appears impossible.

In addition to these arguments, there is an experimental reason for considering near-field effects (i) and (ii) to be relatively small in snow. The experiments of Bohren and Beschta (1979), described in Section 5f, show that the albedo of snow, unlike that of the pigments studied by Blevin and Brown (1961), did not decrease significantly with increasing density (and fixed grain size) up to  $\rho = 0.45 \text{ g cm}^{-3}$ .

## 3) SHADOWING

Shadowing of snow grains by one another reduces the optical depth  $\tau$  as calculated from (1), since all  $N$  grains will not contribute their full cross-section  $\sigma_{\text{ext}}$ . Thus light may penetrate to greater liquid-equivalent depths as snow densifies. On the assumption (which is of course only a crude approximation) that a grain is either completely shadowed or completely unshadowed, neither  $\bar{\omega}$  nor  $g$  would be affected by shadowing. In this case, shadowing would reduce the albedo of a *thin* snowpack only, so it could not account for the discrepancy between theory and observation for semi-infinite snow.

We think it is quite possible that shadowing does reduce the albedo of a thin snowpack. Brillouin [1949, Eq. (5) and Fig. 2], using very crude physical optics considerations, derived that the region of complete shadow (umbra) should extend a distance  $R \sim r^2/2\lambda$  when  $\lambda \ll r$ . According to this criterion, shadowing occurs at all solar wavelengths for all grain sizes and densities present in natural snow. The effect of shadowing has been observed for particles in paint by Blevin and Brown (1961), who commented “. . . very high pigment concentration in a paint layer can cause a decrease in its opacity or hiding power.” Shadowing cannot be ruled out as a potential explanation for the discrepancy between measurement and observation. But the direction of its effect on the albedo of deep snow, and whether it would affect the visible more than the near-IR albedo, is at present not at all clear.

### b. Nonsphericity

Experiments (e.g., Zerull, 1976) have shown that the sphericity assumption is sometimes adequate for describing scattering by ensembles of nonspherical particles. It becomes worse for larger and/or

highly irregular particles. The details of the angular scattering pattern (phase function) are the most sensitive to nonsphericity; generally sidescattering is enhanced while backscattering is depressed relative to spheres. The cross sections for absorption and scattering are likely to be much less sensitive to nonsphericity than is the phase function at specific angles.

Mugnai and Wiscombe (1980) have studied these cross sections theoretically for randomly oriented moderately nonspherical particles and find them to be quite close to those for equal-volume spheres. In the semi-empirical theory of Pollack and Cuzzi (1980), the absorption cross section is unaltered (from its equal-volume sphere value) while the scattering cross section is increased by the ratio

$$r = \frac{\text{total surface area of irregular particles}}{\text{total surface area of equal-volume spheres}}$$

Since

$$1 - \bar{\omega} = \sigma_{\text{abs}}/\sigma_{\text{sca}}$$

to an excellent approximation for snow at  $\lambda \leq 0.9 \mu\text{m}$ , we would have

$$(1 - \bar{\omega})_{\text{nonspherical}} = \frac{1}{r} (1 - \bar{\omega})_{\text{spherical}},$$

according to the Pollack/Cuzzi theory.  $r$  is not likely to be larger than 3 for typical snow grains, and a factor of 3 reduction in  $(1 - \bar{\omega})$  will have little effect (less than 1%) on our visible albedo calculations. But in any case the reduction in  $(1 - \bar{\omega})$  caused by nonsphericity is exactly opposite in direction to what we need; a 50–100-fold increase is required to explain our disagreement with observations.

It might be noted that Hansen and Pollack (1970) assumed ice spheres in modeling the reflectivity of thick ice clouds and found agreement with laboratory measurements even though cloud ice particles are even more irregular than snow grains. Thus the nonsphericity corrections, while certainly real, are probably small.

In a situation similar to ours, near-field and nonsphericity effects were ignored with impunity by Conel (1969). He used the Chandrasekhar two-stream approximation and Mie scattering theory to predict spectral emissivity of mineral dust. He was able successfully to predict many of the IR spectral emissivity features of nonspherical close-packed quartz powders in various states of granulation.

Independent of the above arguments, there is a reason sufficient in itself to show that neither close-packing nor nonsphericity significantly reduces visible snow albedo (except for shadowing in thin snowpacks). Very high values of visible albedo, such as our model predicts, are indeed sometimes observed in dry compact snow. These are the

measurements of Liljequist (1956),  $a_d = 97\%$  at  $\lambda = 0.52 \mu\text{m}$  in Antarctica; and of Bryazgin and Koptev (1969), 93% for 0.4–1.0  $\mu\text{m}$  in the Arctic Ocean. The fact that some measurements of snow albedo approach the theoretical values would cast suspicion on a nonsphericity and/or near-field explanation, since if such mechanisms are operative one cannot expect them to be just intermittently operative.

## 8. Summary and conclusions

Use of Mie theory for single-scattering and the  $\delta$ -Eddington approximation for multiple scattering of solar radiation in a snowpack allows the snow albedo to be calculated over the entire solar spectrum ( $0.3 \leq \lambda \leq 5.0 \mu\text{m}$ ) for diffusely or directly incident radiation at any zenith angle.

The peaks and valleys of the measured spectral albedo of snow coincide with the minima and maxima, respectively, of the measured spectral absorption coefficient. The absorption coefficient of ice is thus a primary determinant of the spectral albedo of snow, and model calculations of spectral albedo can be no better than the measured absorption coefficients used in the model.

Ice is very weakly absorptive in the visible spectrum but has strong absorption bands in the near-infrared so snow albedo is much lower there. The near-IR solar irradiance thus plays an important role in snowmelt and in the energy balance at a snow surface. Furthermore, while the visible albedo (for pure snow) is rather insensitive to variations in model parameters, the near-IR albedo is very sensitive to snow grain size and moderately sensitive to solar zenith angle.

The albedo of a thin snowpack is affected by the underlying surface. The depth necessary for the snow to be "effectively semi-infinite" increases with the grain size; for old melting snow it may be  $\sim 20$  cm liquid equivalent (50 cm snow). Thus, it is important to record the snow depth and density as well as grain size for albedo measurements on snow less than 1 m thick. Snow cover over Arctic sea ice is often thin enough that its albedo may be reduced by the darker underlying ice.

The model calculations agree well with observations in the near-IR. The decrease in albedo due to snow aging can be mimicked by reasonable increases in grain size. In the visible and near-UV, however, the calculated values exceed almost all observed albedos for deep snow. The discrepancy is worst for old melting snow.

Errors due to approximations made by the model cannot explain the discrepancy. The possible adjustments for near-field effects and nonsphericity of snow grains are judged to be an order of magnitude too small to reduce the calculated visible albedo sufficiently. Furthermore, they affect all

wavelengths so that matching of observed visible albedo for a particular grain size would destroy the model's good agreement in the near-IR.

The measured absorption coefficient of ice is unlikely to be in error by more than a factor of 2, whereas a factor of 50 would be needed to bring our high visible albedo calculations down to observed values. (Nevertheless, we would suggest high priority for a remeasurement of the absorption coefficient of pure ice for wavelengths 0.3–2.0  $\mu\text{m}$ .)

We conclude that the model does indeed calculate reasonable albedos for *pure* snow. For natural snow, the measured albedo is often lower (in the visible, but not in the near-IR) than that for pure snow. In Part II of this paper (Warren and Wiscombe, 1980), we attribute this to the presence of absorptive impurities. The best candidate for pure snow would be the Antarctic plateau because of its isolation from contaminants.

*Note added in proof.* Grenfell and Perovich (1981) have now remeasured  $m_{\text{im}}(\text{ice})$  for  $0.4 \leq \lambda \leq 1.4 \mu\text{m}$ , using a 2.3 m long block of ice. The new values differ by at most a factor of 2 from Sauberer's (1950) values. These largest differences are at  $0.4 \leq \lambda \leq 0.6 \mu\text{m}$ ; the minimum in  $m_{\text{im}}$  is now found at 0.47  $\mu\text{m}$  instead of 0.40  $\mu\text{m}$ . These new values are expected to have only minor effects on our calculated albedos (cf. Fig. 14) but will shift the position of maximum albedo to slightly higher wavelength, possibly in better agreement with Liljequist's (1956) observations (cf. Fig. 17).

*Acknowledgments.* We thank Thomas Grenfell and Gary Maykut (U. Washington), Malcolm Mellor (CRREL) and Charles Knight (NCAR) for helpful discussions, and Harold O'Brien (CRREL) for giving us details of his experimental measurements.

#### REFERENCES

- Abramowitz, M., and I. A. Stegun, 1965: *Handbook of Mathematical Functions*. Dover Publications, 1046 pp.
- Arai, T., 1966: On the relationship between albedo and the properties of snow. *Japanese Progress in Climatology*, Tokyo University of Education, 88–95.
- Barkstrom, B. R., 1972: Some effects of multiple scattering on the distribution of solar radiation in snow and ice. *J. Glaciol.*, **11**, 357–368.
- Bergen, J. D., 1971: The relation of snow transparency to density and air permeability in a natural snow cover. *J. Geophys. Res.*, **76**, 7385–7388.
- , 1975: A possible relation of albedo to the density and grain size of natural snow cover. *Water Resour. Res.*, **11**, 745–746.
- Blevin, W. R., and W. J. Brown, 1961: Effect of particle separation on the reflectance of semi-infinite diffusers. *J. Opt. Soc. Amer.*, **51**, 129–134.
- Bode, G., 1909: Das Verhalten des Eises im ultraroten Spektrum. *Ann. Phys.*, **30**, 326–336.
- Bohren, C. F., and B. R. Barkstrom, 1974: Theory of the optical properties of snow. *J. Geophys. Res.*, **79**, 4527–4535.
- , and R. L. Beschta, 1979: Snowpack albedo and snow density. *Cold Regions Sci. Tech.*, **1**, 47–50.
- Born, M., and E. Wolf, 1965: *Principles of Optics*, 3rd ed. Pergamon Press, 808 pp.
- Brillouin, L., 1949: The scattering cross section of spheres for electromagnetic waves. *J. Appl. Phys.*, **20**, 1110–1125.
- Bryazgin, N., and A. Koptev, 1969: Spectral albedo of snow-ice cover. *Prob. Arctic Antarc.*, **29–32**, 355–360.
- Choudhury, B. J., and A. T. C. Chang, 1979: The solar reflectance of a snow field. *Cold Regions Sci. Tech.*, **1**, 121–128.
- Colbeck, S. C., 1975: Grain and bond growth in wet snow. *Snow Mechanics Symposium*, IAHS-AISH Publ. No. 114, 51–61.
- , 1979: Grain clusters in wet snow. *J. Colloid Interface Sci.*, **72**, 371–384.
- Conel, J. E., 1969: Infrared emissivities of silicates: Experimental results and a cloudy atmosphere model of spectral emission from condensed particulate mediums. *J. Geophys. Res.*, **74**, 1614–1634.
- Dirmhirn, I., and F. D. Eaton, 1975: Some characteristics of the albedo of snow. *J. Appl. Meteor.*, **14**, 375–379.
- Dunkle, R. V., and J. T. Bevans, 1956: An approximate analysis of the solar reflectance and transmittance of a snow cover. *J. Meteor.*, **13**, 212–216.
- Gate, L. F., 1973: Light-scattering cross sections in dense colloidal suspension of spherical particles. *J. Opt. Soc. Amer.*, **63**, 312–317.
- Giddings, J. C., and E. R. LaChapelle, 1961: Diffusion theory applied to radiant energy distribution and albedo of snow. *J. Geophys. Res.*, **66**, 181–189.
- Gow, A. J., 1969: On the rates of growth of grains and crystals in South Polar firn. *J. Glaciol.*, **8**, 241–252.
- Grenfell, T. C., 1979: The effect of ice thickness on the exchange of solar radiation over the polar oceans. *J. Glaciol.*, **22**, 305–320.
- and G. A. Maykut, 1977: The optical properties of ice and snow in the Arctic basin. *J. Glaciol.*, **18**, 445–463.
- , and D. K. Perovich, 1981: Radiation absorption coefficients of polycrystalline ice from 400 nm to 1400 nm. Submitted to *J. Geophys. Res.*
- Griggs, M., 1968: Emissivities of natural surfaces in the 8- to 14-micron spectral region. *J. Geophys. Res.*, **73**, 7545–7551.
- Grum, F., and G. W. Luckey, 1968: Optical sphere paint and a working standard of reflectance. *Appl. Opt.*, **7**, 2289–2294.
- Hale, G. M., and M. R. Querry, 1973: Optical constants of water in the 200 nm to 200  $\mu\text{m}$  wavelength region. *Appl. Opt.*, **12**, 555–563.
- Hansen, J. E., and J. B. Pollack, 1970: Near-infrared light scattering by terrestrial clouds. *J. Atmos. Sci.*, **27**, 265–281.
- and L. D. Travis, 1974: Light scattering in planetary atmospheres. *Space Sci. Rev.*, **16**, 527–610.
- Hanson, K., 1960: Radiation measurements on the Antarctic snowfield, a preliminary report. *J. Geophys. Res.*, **65**, 935–946.
- Harding, R. H., B. Golding and R. A. Morgen, 1960: Optics of light-scattering films. Study of effects of pigment size and concentration. *J. Opt. Soc. Amer.*, **50**, 446–455.
- Havens, J. M., 1964: Meteorology and heat balance of the accumulation area, McGill Ice Cap. Axel Heiberg Island Research Reports, Meteorology, No. 2, McGill University, 87 pp.
- Heller, W., 1945: The determination of refractive indices of colloidal particles by means of a new mixture rule or from measurements of light scattering. *Phys. Rev.*, **68**, 5–10.
- Hiltner, P. A., and I. M. Krieger, 1969: Diffraction of light by ordered suspensions. *J. Phys. Chem.*, **73**, 2386–2389.
- Hobbs, P. V., 1974: *Ice Physics*. Oxford, Clarendon Press, 837 pp.
- Holmgren, B., 1971: *Climate and Energy Exchange on a Sub-polar Ice Cap in Summer*. Part E, Radiation Climate.

- Uppsala, Meteorologiska Institutionen Uppsala Universitet, 111 pp.
- Hottel, H. C., A. F. Sarofim, W. H. Dalzell and I. A. Vasalos, 1971: Optical properties of coatings: Effect of pigment concentration. *AIAA J.*, **9**, 1895–1898.
- Hubley, R. C., 1955: Measurements of diurnal variations in snow albedo on Lemon Creek Glacier, Alaska. *J. Glaciol.*, **2**, 560–563.
- Irvine, W. M., and J. B. Pollack, 1968: Infrared optical properties of water and ice spheres. *Icarus*, **8**, 324–360.
- Joseph, J. H., W. J. Wiscombe and J. A. Weinman, 1976: The delta-Eddington approximation for radiative flux transfer. *J. Atmos. Sci.*, **33**, 2452–2459.
- Kalitin, N. N., 1936: The transparency of ice to ultraviolet solar radiation. *Arktic. Inst. Tr.*, **89**, 55–70 [English translation available from Office of Technical Services, U.S. Department of Commerce, Washington, DC].
- Kislovskii, L. D., 1959: Optical characteristics of water and ice in the infrared and radiowave region of the spectrum. *Opt. Spektros.* (English edition), **7**, 201–206.
- Kondratiev, K. Ya., Z. F. Miranova and A. N. Otto, 1964: Spectral albedo of natural surfaces. *Pure Appl. Geophys.*, **59**, 207–216.
- Kuhn, M., and L. Siogas, 1978: Spectroscopic studies at McMurdo, South Pole and Siple Stations during the austral summer 1977–78. *Antarctic J. U.S.*, **13**, 178–179.
- Kukla, G. J., and H. J. Kukla, 1974: Increased surface albedo in the northern hemisphere. *Science*, **189**, 709–714.
- LaChapelle, E. R., 1969: *Field Guide to Snow Crystals*. University of Washington Press, 101 pp.
- Langleben, M. P., 1968: Albedo measurements of an arctic ice cover from high towers. *J. Glaciol.*, **7**, 289–297.
- Liljequist, G. H., 1956: Energy exchange of an Antarctic snowfield. Short-wave radiation (Maudheim, 71°03'S, 10°56'W). *Norwegian-British-Swedish Antarctic Expedition, 1949–52, Scientific Results*, Vol. 2, Pt. 1A, Oslo, Norsk Polarinstitut, 107 pp.
- Luck, W., 1963: Beitrag zur Association des flussigen Wassers. I. *Ber. Bunsengesell. Phys. Chem.*, **67**, 186–190.
- Lyons, J. B., and R. E. Stoiber, 1959: The absorptivity of ice: A critical review. *Sci. Rep. No. 3*, Dartmouth College, 13 pp.
- Mellor, M., 1977: Engineering properties of snow. *J. Glaciol.*, **19**, 15–66.
- Middleton, W. E. K., and A. G. Mungall, 1952: The luminous directional reflectance of snow. *J. Opt. Soc. Amer.*, **42**, 572–579.
- Mugnai, A., and W. J. Wiscombe, 1980: Scattering of radiation by moderately nonspherical particles. *J. Atmos. Sci.*, **37**, 1291–1307.
- Nakaya, V., 1954: *Snow Crystals: Natural and Artificial*. Harvard University Press, 510 pp.
- Ockman, N., 1958: The infrared and Raman spectra of ice. *Advances in Physics*, Vol. 7, Academic Press, 199–220.
- Palmer, K. F., and D. Williams, 1974: Optical properties of water in the near infrared. *J. Opt. Soc. Amer.*, **64**, 1107–1110.
- Patel, C. K. N., and A. C. Tam, 1979: Optical absorption coefficients of water. *Nature*, **280**, 302–304.
- Paterson, W. S. B., 1969: *The Physics of Glaciers*. Pergamon Press, 250 pp.
- Patterson, E. M., C. E. Shelden and B. H. Stockton, 1977: Kubelka-Munk optical properties of a barium sulfate white reflectance standard. *Appl. Opt.*, **16**, 729–732.
- Petzold, D. E., 1977: An estimation technique for snow surface albedo. *Clim. Bull.* (McGill University), **21**, 1–11.
- Pollack, J. B., and J. N. Cuzzi, 1980: Scattering by nonspherical particles of size comparable to a wavelength: A new semi-empirical theory and its application to tropospheric aerosols. *J. Atmos. Sci.*, **37**, 868–881.
- Post, A., and E. R. LaChapelle, 1971: *Glacier Ice*. University of Washington Press, 110 pp.
- Reding, F. P., 1951: The vibrational spectrum and structure of several molecular crystals at low temperature. Ph.D. thesis, Brown University, 147 pp.
- Roulet, R. R., G. A. Maykut and T. C. Grenfell, 1974: Spectrophotometers for the measurement of light in polar ice and snow. *Appl. Opt.*, **13**, 1652–1658.
- Rusin, N. P., 1961: *Meteorologicheskii i radiatsionnyy rezhim Antarktity*. Leningrad, Gidrometeorologicheskoye Izdatel'stvo. [English translation: *Meteorological and Radiation Regime of Antarctica*. Jerusalem, Israel Program for Scientific Translations, 1964, 355 pp.]
- Sarofim, A. F., H. C. Hottel and E. J. Fahimian, 1968: Scattering of radiation by particle layers. *AIAA J.*, **6**, 2262–2266.
- Sauberer, F., 1938: Versuche uber spectrale Messungen der Strahlungseigenschaften von Schnee und Eis mit Photoelementen. *Meteor. Z.*, **55**, 250–255.
- , 1950: Die spektrale Strahlungsdurchlässigkeit des Eises. *Wetter und Leben*, **2**, 193–197.
- Schaaf, J. W., and D. Williams, 1973: Optical constants of ice in the infrared. *J. Opt. Soc. Amer.*, **63**, 726–732.
- Schlatter, T. W., 1972: The local surface energy balance and subsurface temperature regime in Antarctica. *J. Appl. Meteor.*, **11**, 1048–1062.
- Schwerdtfeger, P., 1969: Absorption, scattering and extinction of light in ice and snow. *Nature*, **222**, 378–379.
- Siegel, R., and J. R. Howell, 1972: *Thermal Radiation Heat Transfer*. McGraw-Hill, 814 pp.
- Sommerfeld, R. A. and E. LaChapelle, 1970: The classification of snow metamorphism. *J. Glaciol.*, **9**, 3–17.
- Stephenson, P. J., 1967: Some considerations of snow metamorphism in the Antarctic ice sheet in the light of ice crystal studies. *Physics of Snow and Ice*, H. Oura, Ed., *Proc. Int. Conf. Low Temperature Sciences*, 14–19 August 1966, Sapporo, Japan, Bunyeido Printing Company, 725–740.
- Strong, A. E., E. P. McClain and D. F. McGinnis, 1971: Detection of thawing snow and ice packs through the combined use of visible and near-infrared measurements from earth satellites. *Mon. Wea. Rev.*, **99**, 828–830.
- Tam, A. C., and C. K. N. Patel, 1979: Optical absorptions of light and heavy water by laser optoacoustic spectroscopy. *Appl. Opt.*, **18**, 3348–3358.
- van de Hulst, H. C., 1957: *Light Scattering by Small Particles*. Wiley, 470 pp.
- Vedernikova, E. A., and M. V. Kabanov, 1974: Scattering of optical radiation by a system of closely spaced scatterers. *Opt. Spectrosc.*, **37**, 71–74.
- Warren, S. G., and W. J. Wiscombe, 1980: A model for the spectral albedo of snow. II. Snow containing atmospheric aerosols. *J. Atmos. Sci.*, **37**, 2734–2745.
- Weller, G., 1968: Heat-energy transfer through a four-layer system: Air, snow, sea ice, sea water. *J. Geophys. Res.*, **73**, 1209–1220.
- , 1969: Radiation diffusion in Antarctic ice media. *Nature*, **221**, 355–356.
- Wiscombe, W. J., 1977: The Delta-Eddington approximation for a vertically inhomogeneous atmosphere. NCAR Tech. Note 121 [NTIS P6270618].
- , 1979: Mie scattering calculations: Advances in technique and fast, vector-speed computer codes. NCAR Tech. Note TN-140+STR [NTIS PB 301388].
- , 1980: Improved Mie scattering algorithms. *Appl. Opt.*, **19**, 1505–1509.
- , and J. H. Joseph, 1977: The range of validity of the Eddington approximation. *Icarus*, **32**, 362–377.
- Zerull, R. H., 1976: Scattering measurements of dielectric and absorbing nonspherical particles. *Beitr. Phys. Atmos.*, **49**, 166–168.